



Magma residence and eruption at the Taupo Volcanic Center (Taupo Volcanic Zone, New Zealand): insights from rhyolite-MELTS geobarometry, diffusion chronometry, and crystal textures

Ayla S. Pamukçu¹ · Kylie A. Wright² · Guilherme A. R. Gualda² · Darren Gravley³

Received: 1 April 2019 / Accepted: 6 April 2020 / Published online: 21 April 2020
© Springer-Verlag GmbH Germany, part of Springer Nature 2020

Abstract

The Taupo Volcanic Center [TVC; Taupo Volcanic Zone (TVZ), New Zealand] is home to the two most recent silicic caldera-forming eruptions in the TVZ—the giant (530 km³ DRE) Oruanui supereruption and the large (35 km³ DRE) Taupo eruption. This offers a unique opportunity to investigate similarities and differences between large and supersized volumes of rhyolitic magma at the TVC and more generally. We combine information from crystal textures (crystal size distributions), crystal compositions (Ti-in-quartz diffusion chronometry), and glass compositions (rhyolite-MELTS geobarometry) to investigate the crustal storage conditions, longevity, and eruption of these magmas. Results show differences between the storage depths of the Oruanui and Taupo magmas consistent with the differences in their glass silica contents but strikingly similar, short crustal residence times for the final crystal-poor, eruptible magma bodies (decades to centuries). Differences in groundmass textures between the two systems also likely reflect differences in ascent durations, decompression paths, and/or amounts of undercooling experienced by these systems due to the differences in their storage depths. Finally, comparing the evolution of storage depths and magma compositions at the TVC with those in a preceding central TVZ ignimbrite ‘flare-up’ supports the idea that the modern TVC may be flaring up and highlights the evolution of magma storage depths with increasing system maturity in this volcanic region.

Keywords Oruanui · Taupo · Residence time · Decompression · Storage pressure

Communicated by Mark S. Ghiorso.

Electronic supplementary material The online version of this article (<https://doi.org/10.1007/s00410-020-01684-2>) contains supplementary material, which is available to authorized users.

✉ Ayla S. Pamukçu
apamukcu@stanford.edu

Kylie A. Wright
kylie.wright@vanderbilt.edu

Guilherme A. R. Gualda
g.gualda@vanderbilt.edu

Darren Gravley
darren.gravley@canterbury.ac.nz

¹ Geological Sciences, Stanford University, 450 Jane Stanford Way, Bldg. 320, Stanford, CA 94305, USA

² Department of Earth and Environmental Sciences, Vanderbilt University, PMB 351805, 2301 Vanderbilt Place, Nashville, TN 37235, USA

³ Geological Sciences, University of Canterbury, Private Bag 4800, Christchurch, New Zealand

Introduction

Rhyolitic magmas have produced some of the most explosive and voluminous volcanic eruptions in Earth’s history and such evolved magmas dominate in the continental crust. Consequently, efforts to constrain how long and where these magmas reside in the crust, as well as the causes, timing, duration, and path over which they ultimately erupt, are important both for future volcanic hazards management and for understanding the formation and evolution of the continental crust. Information on these parameters and processes can be mined from the compositions and textures of crystals, bubbles, and glass; however, interpreting records in the broader context of magma system evolution and eruption are challenged by differences in phase stability, method resolution limits, and overprinting of information by pre-, syn-, and post-eruptive processes. Consequently, it is critical to understand the limitations of a given phase or method for addressing a particular question, and integrating data from multiple materials and/or methods can help minimize

these issues and can be a powerful approach to investigating questions.

In this study, we combine information from crystal textures (crystal size distributions), crystal zoning (diffusion chronometry), and glass compositions (rhyolite-MELTS geobarometry) to investigate the storage conditions, longevity, and eruption of two rhyolitic systems from the Taupo Volcanic Center (TVC) in the Taupo Volcanic Zone (TVZ) in the North Island of New Zealand—the $\sim 530 \text{ km}^3$ DRE, 25.4 ka Oruanui supereruption (Wilson 2001; Vandergoes et al. 2013) and the $\sim 35 \text{ km}^3$ DRE, 1.72 ka Taupo eruption (Wilson and Walker 1985; Hogg et al. 2012). Despite being the two largest eruptions from the TVC and the most recent caldera-forming eruptions in the TVZ, their volumes differ by an order of magnitude, and they likely came from substantially different magmatic systems (Wilson et al. 2006; Barker et al. 2015). Consequently, we investigate not only conditions and processes specific to each of these systems, but also the similarities and differences between large and supersized volumes of rhyolitic magma at the TVC and in the Modern TVZ ($\sim 61 \text{ ka}$ to present; Wilson et al. 2009) more broadly.

The Taupo Volcanic Center

The TVZ is a NE–SW trending rifted arc in the North Island of New Zealand that is driven by the subduction of the Pacific plate beneath the North Island (Fig. 1; Wilson et al.

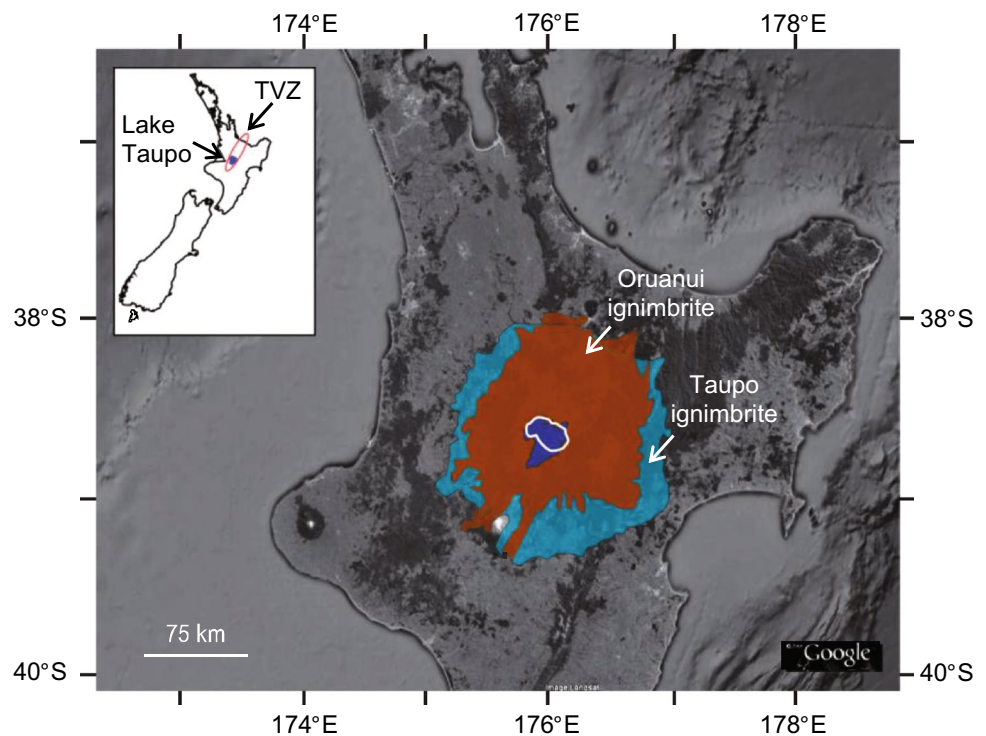
1995). Andesitic cone volcanoes predominate in northern and southern regions, while the central TVZ has dominantly incurred large, explosive, caldera-forming silicic volcanism for the past $\sim 1.6 \text{ Ma}$ (see Wilson et al. 1995 for reviews). During this time, $> 6000 \text{ km}^3$ of rhyolite has erupted from the area (Wilson et al. 2009).

The TVC, located in the central TVZ (Fig. 1), has been intermittently active since $\sim 61 \text{ ka}$ (Wilson et al. 2009) and was “hyperactive” (Barker et al. 2015) for a period of $\sim 24 \text{ ka}$, bookended by the 25.4 ka Oruanui supereruption and the 1.72 ka Taupo eruption. Between these caldera-forming eruptions were 26 smaller ($< 10 \text{ km}^3$ of magma erupted) dacite and low- to moderate-silica rhyolite eruptions. Compositionally, the post-Oruanui rhyolites—delineated into three subgroups (SG; Wilson 1993)—are distinct from Oruanui rhyolites, and it has been suggested that the TVC was destroyed and reconstructed after the Oruanui eruption, with the only similarity between the Oruanui and post-Oruanui magmas being their mafic underpinnings (Barker et al. 2015).

The Oruanui magmatic system

The phreatomagmatic Oruanui eruption is the youngest known supereruption in Earth’s history. It spewed $\sim 530 \text{ km}^3$ of magma (DRE) through a ‘proto’-Lake Taupo (Self and Sparks 1978), ultimately producing 430 km^3 of fall deposits, 320 km^3 of pyroclastic density currents, and 420 km^3 of intracaldera material (Wilson 2001). Subsequent

Fig. 1 Map of the Taupo Volcanic Center, Lake Taupo, and ignimbrite distributions. The NW–SE oriented Oruanui structural caldera is outlined in white; the orange shaded area shows the distribution of the Oruanui ignimbrite. The 1.8 ka Taupo eruption-forming caldera is nested within the Oruanui structure and submerged beneath the northwestern part of the lake; the blue shaded area shows the widespread distribution of the Taupo ignimbrite. Inset: overview map of New Zealand showing the location of the TVZ and Lake Taupo in the North Island



lake formation and post-eruptive landscape-sedimentary response (Manville and Wilson 2004), as well as the later 1.8 ka Taupo eruption (Wilson et al. 1980), have obscured the Oruanui structural caldera beneath the modern Lake Taupo (Fig. 1).

Wilson (2001) discerned ten distinct phases of coeval fall and flow deposition in a detailed stratigraphic study of the Oruanui deposits. The eruption is estimated to have lasted from several months to a year, with an extended time break of weeks to months between eruptive phases 1 and 2 and a few short time breaks (hours to days) between subsequent eruptive phases (Wilson 2001). Presently exposed Oruanui outcrops are comprised of non-welded extracaldera fall and flow material. The deposit is predominantly (99%) rhyolitic in bulk composition (71.8–76.7 wt% SiO₂, anhydrous basis), with much of this high-silica rhyolite (74–76 wt% SiO₂; Wilson 2001) containing 3–13 wt% crystals of plagioclase + quartz + orthopyroxene + hornblende + magnetite + ilmenite + apatite + zircon (Wilson 2001; Charlier et al. 2008). The remaining 1% consists of rare mafic (andesite to basaltic andesite, 52.3–63.3 wt% SiO₂), and still rarer mingled (61.0–74.7 wt% SiO₂), pumice clasts. Allan et al. (2012) also noted biotite-bearing lapilli in phase 1 and 2 deposits, and Allan et al. (2013) identified quartz-free low-silica rhyolite (<74 wt% SiO₂) pumice clasts in phase 3 and 6 deposits.

Compositional variations attributed to simple crystal fractionation are evident in rhyolitic pumice throughout the deposit (Charlier et al. 2008); however, there is no relationship between composition and eruptive phase (Wilson et al. 2006) and no field evidence to suggest the Oruanui eruption systematically tapped a vertically-zoned magma body. Rather, Wilson et al. (2006) suggested that the Oruanui magma was mixed prior to or during the eruption, and/or that the vent position moved during the eruption and tapped compositionally distinct areas of the magma body. Allan et al. (2013, 2017) further suggested that the dominant high-silica rhyolite magma was derived from a thermally and compositionally zoned crystal mush that was only quartz-saturated at the top; they suggest the quartz-free low-silica rhyolite pumice in phase 3 and 6 deposits came from melt deeper in this mush that was evacuated during the eruption. Allan et al. (2012) also surmised that the biotite-bearing lapilli in phase 1 and 2 deposits were derived from a distinct magma that was transported laterally from the northeastern dome system (Sutton et al. 1995) and mixed with the main Oruanui high-silica rhyolite melt during the eruption; the presumed rifting event associated with this lateral migration process (Allan et al. 2012) is also suggested as an explanation for the stop-start nature of the Oruanui eruption.

A handful of studies have investigated crustal storage depths for the Oruanui magma. Liu et al. (2007) and Myers et al. (2018) estimated pressures of ~90–190 MPa

(~3.5–7 km) and ~140–190 MPa, respectively, using H₂O–CO₂ solubilities in quartz-hosted melt inclusions from multiple eruptive phases. Allan et al. (2013, 2017) obtained pressure estimates from amphibole geothermobarometry and amphibole and orthopyroxene stabilities and suggested the Oruanui magma accumulated at ~90–140 MPa (~3.5–6 km) after extraction from a deeper crystal mush at ~140–300 MPa (~6–12 km). Rhyolite-MELTS glass geobarometry applied to Oruanui quartz-hosted melt inclusion compositions by Bégué et al. (2014b) gave pressures of ~45–240 MPa (~1.7–9 km).

Until recently, the longevity of the Oruanui magmatic system was primarily estimated from zircon geochronology. Charlier et al. (2005), using multi-crystal U–Th TIMS and single-crystal U–Th SIMS zircon geochronology, suggested that accumulation of the Oruanui magma occurred between ~2.5 and ~40 ka prior to the eruption, though the compositional evolution of the system leading to magmas with ‘Oruanui-like’ compositions likely took place over the course of ~100 ka. A bimodal age spectrum for the Oruanui, where the oldest age was that of the pre-Oruanui ~30 ka Okaia eruption, was found in subsequent single-crystal U–Th SIMS analyses by Wilson and Charlier (2009), and they revised the longevity of the Oruanui magma to ≤3 ka (i.e., the time between the Okaia and Oruanui eruptions). Allan et al. (2017), using Fe–Mg diffusion chronometry in orthopyroxene crystals, suggested that the eruptible Oruanui magma was extracted from an underlying source crystal mush at most 1.6 ka prior to eruption, with the period of peak extraction occurring a mere 80 a prior to eruption. Timescales from faceting of quartz-hosted melt inclusions are similar and suggest that the final crystal-poor, melt-rich eruptible Oruanui magma crystallized over a period of decades to centuries (Pamukcu et al. 2015b).

The Taupo magmatic system

The Taupo eruption, whose caldera is nested within the western part of the larger Oruanui structure and submerged beneath the lake, deposited ~35 km³ of magma (DRE) in the form of ~13 km³ of fall and ~32 km³ of flow deposits (Wilson and Walker 1985). The two week-long eruption involved six different eruptive phases and multiple vents (Wilson and Walker 1985; Wilson 1993; Smith and Houghton 1995; Barker et al. 2015). Taupo deposits are predominantly low-silica rhyolite (~73–74 wt% SiO₂; Sutton et al. 1995, 2000), and pumice has extremely low crystal contents (~2–5 wt%; Barker et al. 2015) with a phenocryst assemblage of plagioclase + orthopyroxene + magnetite + ilmenite ± quartz (Saunders 2009; Houghton et al. 2010; Barker et al. 2015). Similar to Oruanui, Taupo deposits show no systematic compositional variation with eruptive phase (Dunbar et al. 1989a, b; Sutton et al. 1995; Barker et al. 2015).

In terms of storage pressures, Saunders (2009) calculated values of < 150 MPa from H₂O and CO₂ contents of orthopyroxene- and plagioclase-hosted melt inclusions, and Bégué et al. (2014b) calculated similar pressures (~ 140–180 MPa) using rhyolite-MELTS geobarometry on three quartz-hosted melt inclusions. Smith et al. (2005) projected glass compositions on the haplogranitic ternary and calculated a much deeper crystallization pressure (~ 250 MPa); however, they note that a lack of quartz in their samples makes these pressure estimates only relative ones.

Dunbar and Kyle (1993) suggested a residence time of less than 22 ka for the Taupo magma, because its composition was markedly different from that of Oruanui (at the time dated to 22.59 ka). Using whole-rock, glass, and mineral geochemistry of the Oruanui and post-Oruanui deposits, Sutton et al. (1995, 2000) and Smith et al. (2005) subsequently suggested that the Taupo magma was not present in the crust at any time coincident with the Oruanui magma, or even as late as the post-Oruanui 3.6 ka Waimahia eruption (eruption unit S; Wilson 1993; Sutton et al. (2000) ultimately proposed a residence time of ~ 1 ka for the Taupo magma. They also hypothesized that the Taupo and Oruanui magmas came from different sources and magmatic systems because the SG2 and SG3 rhyolites (including Taupo) were compositionally distinct from both the Oruanui and SG1 rhyolites. Barker et al. (2014, 2015, 2016) further posited that the Taupo magma did not form until after the post-Oruanui SG2 rhyolite eruptions (~ 7–2.8 ka) and that the maximum residence time for the Taupo magma would be 0.01–1 ka. However, unlike the previous studies, Barker et al. (2015, 2016) suggest that the compositional differences in SG rhyolites are due to changes in crystallization conditions over time (i.e., not a change in the magma source and system).

Materials and methods

Samples

Descriptions and GPS locations of the samples collected and analyzed for this study can be found in Table 1. Most Oruanui samples were collected during two field sessions in 2012, and Taupo samples were collected during field sessions in 2012 and 2013. Five additional Oruanui samples (P15xx) were part of the sample set detailed by Wilson (2001) and were provided to us by A. T. Anderson Jr.; a subset of these were also used by Liu et al. (2007) and Pamukcu et al. (2015b). The ORUA samples were also used by Bégué et al. (2014b).

We also use matrix glass and melt inclusion compositional data from the literature (Allan et al. 2013, 2017; Bégué et al. 2014b; Saunders 2009; Liu et al. 2007; Myers et al. 2018; Barker et al. 2015). These include data on

samples from a variety of eruptive phases in both eruptions; details and descriptions of these samples can be found in the respective publications.

Rhyolite-MELTS geobarometry and glass compositions

Rhyolite-MELTS glass geobarometry (Gualda and Ghiorso 2014) utilizes rhyolite-MELTS (Gualda et al. 2012) to assess crystallization pressures from glass (matrix or melt inclusion) in silicic rocks containing quartz and feldspar. The geobarometer operates by running rhyolite-MELTS crystallization simulations over a range of pressures and finds the pressure at which a melt of a given composition is in equilibrium with a mineral assemblage that includes quartz and feldspar. Results from the rhyolite-MELTS geobarometer have been shown to agree well with independent estimates of pressure (e.g., haplogranitic ternary, volatile solubility, amphibole geobarometry; Gualda and Ghiorso 2014; Bégué et al. 2014a, b; Pamukcu et al. 2015a; Gualda et al. 2019).

We use rhyolite-MELTS to determine saturation temperatures for quartz and feldspar (as well as other phases, which are not used in the pressure calculation) as a function of pressure for a given matrix or melt inclusion glass composition. The pressure of interest is that at which at least two phases (quartz, plagioclase, and/or sanidine) are simultaneously saturated at the liquidus temperature for that composition.

Following the methods outlined by Gualda and Ghiorso (2014), we ran a total of 893 glass compositions (655 Oruanui, matrix glass and quartz-hosted melt inclusions; 238 Taupo, matrix glass only) with the rhyolite-MELTS geobarometer. Of these, 463 were new matrix glass compositions that we determined at Vanderbilt University (Nashville, TN) using an Oxford X-max 50 mm² EDS attached to a Tescan Vega 3 LM Variable Pressure SEM. Accelerating voltages of 15 kV and absorbed currents of ~ 2.5 nA were used to scan analysis areas of > 10 μm² for 30 s. To minimize Na loss, we used live acquisition times of 15 s, with a deadtime of ~ 50–60%, which results in total analytical times of ~ 30 s; our tests show minimal changes in Na contents of reference rhyolitic glasses under these conditions. A fused USGS rhyolite glass standard (RGM-1) was analyzed during each session to check the quality of the analytical procedure. The remaining 429 compositions were those published previously by Bégué et al. (2014b; 25 melt inclusion), Allan et al. (2013, 2017; 174 matrix glass, 65 melt inclusion), Saunders (2009; 11 matrix glass, 21 melt inclusion), Liu et al. (2007; 7 melt inclusion), Myers et al. (2018; 98 melt inclusion) and Barker et al. (2015; 29 matrix glass). All compositions and RGM-1 analyses can be found in Supplementary Material 1.

The range of temperatures and pressures we investigated with the geobarometer was 1000–700 °C in 1 °C

Table 1 Sample locations, descriptions, and analyses performed

Sample name	GPS location ^a	Eruptive phase ^b	Analyses ^c	Notes ^d
ORN-018	38° 36' 56.07" S 175° 52' 24.73" E	Unknown	r-MELTS	Collected in 2012
ORN-019	38° 40' 47.67" S 175° 41' 14.90" E	Type E Ignimbrite	r-MELTS	Collected in 2012
ORN-021	38° 35' 50.58" S 175° 58' 41.82" E	10	r-MELTS	Collected in 2012
ORN-052_A,B	38° 39' 26.07" S 176° 01' 42.04" E	1	r-MELTS	Collected in 2012 at 2288 locality
ORN-061_C	38° 47' 14.30" S 175° 41' 9.70" E	Unknown (possibly 6)	r-MELTS	Collected in 2012, south of 1944 and 1952 localities, on Highway 32
ORN-066_B	38° 55' 52.79" S 176° 06' 33.21" E	6	r-MELTS	Collected in 2012 at 1513 locality
ORN-067	38° 57' 37.14" S 176° 03' 19.24" E	10	r-MELTS, CSD, CL	Collected in 2012 at 1511 locality
ORN-069	38° 56' 49.68" S 176° 00' 39.61" E	10	r-MELTS	Collected in 2012 at 737 locality
P1537	38° 56' 3.55" S 176° 00' 58.01" E	10	r-MELTS, CSD	Originally collected by Wilson at locality 1580; H ₂ O–CO ₂ pressures determined previously (Liu et al. 2006)
P1541	38° 56' 3.55" S 176° 00' 58.01" E	10	r-MELTS, CSD	Originally collected by Wilson at locality 1580; H ₂ O–CO ₂ pressures determined previously by Liu et al. (2006)
P1542	38° 56' 3.55" S 176° 00' 58.01" E	10	r-MELTS, CSD	Originally collected by Wilson at locality 1580; H ₂ O–CO ₂ pressures determined previously (Liu et al. 2006)
P1573	Unknown	1	r-MELTS, CSD	Originally collected by Wilson; H ₂ O–CO ₂ pressures determined previously (Liu et al. 2006)
P1577	Unknown	1	r-MELTS, CSD	Originally collected by Wilson; H ₂ O–CO ₂ pressures determined previously (Liu et al. 2006)
ORUA-48	38° 39' 32.12" S 176° 01' 44.52" E	1 or 2	r-MELTS	Collected in 2012
ORUA-49	38° 39' 32.12" S 176° 01' 44.52" E	1 or 2	r-MELTS	Collected in 2012
ORUA-50	38° 39' 32.12" S 176° 01' 44.52" E	1 or 2	r-MELTS	Collected in 2012
ORUA-51	38° 39' 32.12" S 176° 01' 44.52" E	1 or 2	r-MELTS	Collected in 2012
ORUA-52	38° 39' 32.12" S 176° 01' 44.52" E	1 or 2	r-MELTS	Collected in 2012
TP-IGN, IGN1, IGN3	38° 56' 38.05" S 176° 30' 16.96" E	Taupo ignimbrite	r-MELTS, CSD	Collected in 2012
TP-PLI, PLI1	38° 44' 51.43" S 176° 11' 59.08" E	Taupo plinian	r-MELTS, CSD	Collected in 2012
TP-JET1, JET2	39° 3' 25.18" S 175° 34' 59.85" E	Taupo jetted	r-MELTS, CSD	Collected in 2012

^aGPS locations use WGS 1984 datum

^bEruptive phases as documented by Wilson (2001)

^cr-MELTS: rhyolite-MELTS geobarometry, CSD: crystal size distribution, CL: diffusion chronometry

^dNumbered localities are those of Wilson et al. (2006)

steps and 25–400 MPa in 25 MPa steps. Oxygen fugacity was kept at the Ni–NiO buffer. Water was added to each composition to ensure water-saturation, but the results are not particularly sensitive to water contents (Gualda and Ghiorso 2014; Ghiorso and Gualda 2015).

For Oruanui, which contains quartz and only one feldspar (plagioclase), the relevant saturation condition from our simulations is quartz + 1feldspar (Q1F). For Q1F results, 2 σ errors are 50 MPa (Gualda and Ghiorso 2014). In the case of Taupo, plagioclase is always present and quartz has only

been identified in some units. Consequently, although successful Taupo simulations did result in Q1F estimates, those from units that have not been demonstrated to contain quartz should be taken as maximum pressures. It is worth noting that most Taupo samples are very crystal-poor ($\sim 2\text{--}5$ wt% crystals; Barker et al. 2015); thus, if quartz is rare it may be especially difficult to find without assessing an enormous amount of sample. This is consistent with the fact that the units that did provide quartz (Taupo Ignimbrite) are some of the most crystalline; this was the same for Saunders (2009), who found quartz in the Taupo Ignimbrite layer 1(H) (50% crystals; see Wilson and Walker 1982 for depositional facies nomenclature), the main part of the ignimbrite (layer 2, 2% crystals), and the Hatepe Plinian unit (5% crystals), but not in the Taupo Plinian unit (1% crystals). Houghton et al. (2010), who studied hundreds of Taupo pumice clasts, found quartz in the mineral assemblage as well, but they do not discriminate the exact units in which it was identified.

Timescales and growth rates

Crystal size distributions

We determined crystal size distributions (CSDs) for 11 pumice clasts (6 Oruanui, 5 Taupo) using X-ray tomography on multiple pumice chips per sample, following the methods described by Pamukcu and Gualda (2010). All tomographic imaging was performed at the GSECARS-13 BMD beamline at the Advanced Photon Source (APS) of Argonne National Laboratory (Chicago, IL). The experimental setup is described in detail by Rivers et al. (1999), Gualda and Rivers (2006), and Gualda et al. (2010). Textures of major mineral phases (plagioclase, quartz, magnetite, ilmenite, amphibole, orthopyroxene) were quantified using standard absorption-contrast X-ray tomography (Gualda and Rivers 2006), while differential absorption methods (Gualda et al. 2010) were used for accessory phases (zircon). Size, shape, and position parameters for individual crystals were determined during image processing using the program Blob3D (Ketcham 2005).

In our samples, accessory minerals (zircon), Fe–Ti oxides (magnetite, ilmenite), tectosilicates (quartz, plagioclase), pyroxenes, amphiboles, glass, and air can be separated from one another in tomographic images with confidence. In some cases, the difference in linear attenuation coefficient (i.e., grayscale values in tomographic images) of two phases within or between these groups is slight, making it challenging or impossible to distinguish them during image processing. Here, this issue arises in separating plagioclase from quartz and magnetite from ilmenite, so we assess CSDs for plagioclase + quartz and magnetite + ilmenite in combination (see Pamukcu et al. 2012). Given that feldspar is much more abundant than quartz and magnetite is more abundant than

ilmenite in our samples, we do not expect this approach to substantially impact our timescale estimates from these data (see Gualda and Rivers 2006). Distinguishing zircon from oxides in absorption-contrast tomograms can also be challenging, so we used known positions of zircon crystals from differential absorption tomograms (3D Zr maps; Gualda et al. 2010) to identify and distinguish them from oxides in absorption-contrast tomograms.

CSDs are typically displayed on semi-logarithmic plots of crystal size (here, maximum crystal axis length in μm) versus population density (number of crystals per sample mass per bin size). We calculate timescales from the slopes of CSDs using the relationship $\text{CSD slope} = -1/[\text{growth rate (m/s)} \times \text{time (s)}]$. Main sources of error on these estimates are due to uncertainties associated with counting crystals on the CSD and in the growth rates. While the latter uncertainties can be especially large, and growth rates can vary during crystallization, we use conservative estimates and consider a wide range (two orders of magnitude) of values in our calculations; thus, the errors on our timescales from CSDs are likely smaller than the range of growth rates we use. We discuss our choice of growth rates in more detail in the Discussion. We focus on data from plagioclase + quartz, magnetite + ilmenite, and zircon because growth rate estimates for these phases are available in the literature. For more details about CSD theory and its application to geologic questions, see the treatises of Marsh (1988, 1998).

Diffusion chronometry

Oruanui samples contain abundant quartz, and we assessed timescales and quartz growth rates using Ti diffusion chronometry in quartz from a phase 10 sample (ORN-067). We used cathodoluminescence (CL) intensity as a proxy for Ti (Wark and Watson 2006; Leeman et al. 2012; Gualda et al. 2012; Gualda and Sutton 2016) because CL imaging is faster, less destructive, and results in images with higher spatial resolution than those from other approaches (e.g., X-ray microprobe; Gualda and Sutton 2016; Pamukcu et al. 2016; Gualda et al. 2018). We focus on large gradients in CL intensity, which have been demonstrated to correlate well with variations in Ti content in quartz from other high-silica rhyolite systems (Wark and Watson 2006; Gualda et al. 2012; Matthews et al. 2012; Gualda and Sutton 2016); the correlation is less clear for finer, subtler oscillatory zoning (see Gualda et al. 2012; Pamukcu et al. 2015b). In all cases, we assume that the profiles we are collecting are diffusion profiles, rather than profiles formed due to rapid crystal growth. Evidence in support of this interpretation includes a lack of: (a) zoning patterns consistent with rapid crystal growth, (b) enrichment in Ti contents of crystal rims (which may be due to boundary layer entrapment during rapid crystal growth; Pamukcu et al. 2015a, b), and (c) a microlite

population that would be expected under circumstances that also favor fast crystal growth (e.g., decompression). In the case that these are growth, rather than diffusion, profiles, the results do not change our interpretation—they still provide us with a maximum time estimate.

CL images of quartz crystals were obtained with a Tescan CL detector attached to a Tescan Vega 3 LM Variable Pressure SEM at Vanderbilt University, using a beam energy of 15 keV and beam intensity of 19 (~2.5 nA absorbed current). Pamukcu et al. (2015b) showed that a 5–15 keV beam produces the best signal-to-noise ratio in CL images used for diffusion chronometry, and Gualda and Sutton (2016) showed that a beam energy of 5 kV or lower is ideal for diffusion chronometry, particularly for short gradients (i.e., < 1 μm). In the case of Oruanui quartz, however, variations in CL intensity can be subtle, and imaging is not always practical at these low energies. Consequently, we adopted a 15 kV beam energy for the CL profiles collected here. This approach results in lower spatial resolution in our images and some smoothing of the profiles; however, this only results in overestimates of our calculated timescales and growth rates. Our use of a 15 kV beam energy results in a spatial resolution of ~1 μm (Gualda and Sutton 2016). Using the formalism of Bradshaw and Kent (2017), we calculate that under these conditions the minimum timescale that we can accurately resolve is ~2–14 years at the temperatures we consider in this study (see below), and we only use those analyses that resulted in timescales equal to or greater than these values in our discussion. Grain orientation also impacts the effective thickness of a growth zone, which can affect growth rate estimates, so we made concerted efforts to orient crystals parallel to the *c*-axis and expose their centers for imaging. In cases where we did not achieve this, the growth rates would be maximally slow, because off-axis orientations would result in an apparent zone thickness that is greater than the true thickness.

Whole crystals were initially imaged with fast scan speeds (0.1–0.3 ms/pixel) to obtain a reference image while minimizing beam damage to the sample. Boundaries of interest found in these images were then scanned in more detail using ~0.2 μm /pixel resolution and acquisition times of 1 ms/pixel. Eleven parallel grayscale intensity profiles, spaced in one-pixel intervals (five on each side of the original profile), were obtained from these details using `img_profile` (see Gualda and Sutton 2016), one of the programs in the `img_tools` image processing software package (https://my.vanderbilt.edu/ggualda/img_tools/).

Similar to the approach of Gualda et al. (2012), Pamukcu et al. (2015b), and Gualda and Sutton (2016), we use least-square minimization to determine the complementary error function that best fits the observed profile. We estimated timescales from each individual profile and from an average profile, which was obtained by averaging the individual

profiles. We assume the initial profile was a step-function, so calculated times are maxima (see Gualda et al. 2012). We also calculate average growth rates using the relationship Average Growth Rate = Length/Time, where ‘Length’ is the distance between the zone boundary of interest and the nearest crystal edge, and ‘Time’ is that calculated for the relevant boundary (see Pamukcu et al. 2015b; Gualda and Sutton 2016). Both parameters are determined using `img_tools`. We calculate Ti diffusivity in quartz using the equation of Cherniak et al. (2007) and a temperature of 770 °C (Allan et al. 2013). Errors on time estimates are on the order of 100% (Gualda et al. 2012); this takes into account uncertainties on temperature (T ; ± 30 °C, a reasonable range for eutectoid systems), the activation energy for diffusion (E ; ± 12 kJ/mol, determined experimentally), a pre-exponential factor ($\ln[D_0]$; ± 0.525 , determined experimentally), and the characteristic diffusion length scale (L ; 10–50%, estimated from Monte Carlo modeling of each point along L).

Rhyolite-MELTS decompression simulations

To investigate the effect of liquidus temperatures on decompression crystallization, we ran isothermal and adiabatic rhyolite-MELTS decompression crystallization simulations. Starting compositions were average whole-rock phase 1 and phase 10 Oruanui compositions (Wilson et al. 2006) and Taupo Initial Ash and Taupo Ignimbrite compositions (Barker et al. 2015). For Oruanui simulations, we explored the range 140–25 MPa at 835 °C (phase 1) and 825 °C (phase 10). For Taupo simulations, we considered the range 330–25 MPa at 761 °C (Taupo Initial Ash; phase 1) and 766 °C (Taupo Ignimbrite; phase 7). These temperatures represent the liquidus at the start of the simulation (i.e., at high pressure); we thus assume there were no crystals present at the start of decompression, which is a conservative estimate.

Results

Glass compositions

Of the 894 glass analyses input into the rhyolite-MELTS geobarometer, 745 (528 Oruanui, 217 Taupo) resulted in Q1F pressures (Figs. 2, 3, Supplementary Material 1). Following the approach used in other studies (Gualda and Ghiorso 2013, 2014; Bégué et al. 2014a, b; Pamukcu et al. 2015a), we removed glass compositions from the dataset if they did not return a pressure estimate. We consider these compositions to be erroneous or compromised due to issues such as analytical imprecision, a lack of equilibrium between the phenocryst assemblage and the glass (i.e., the phenocryst assemblage does not reflect the equilibrium assemblage), or

Fig. 2 SiO₂ vs. Na₂O contents of all Oruanui glass compositions. Literature compositions are those with author names in parentheses. Filled symbols = Matrix glass. Open symbols = Melt inclusion (MI). (Top) All compositions that gave rhyolite-MELTS pressures. (Bottom) The final dataset after outliers were removed. Error bars on new data (filled color circles) are 2σ uncertainties; those not visible are smaller than the symbol

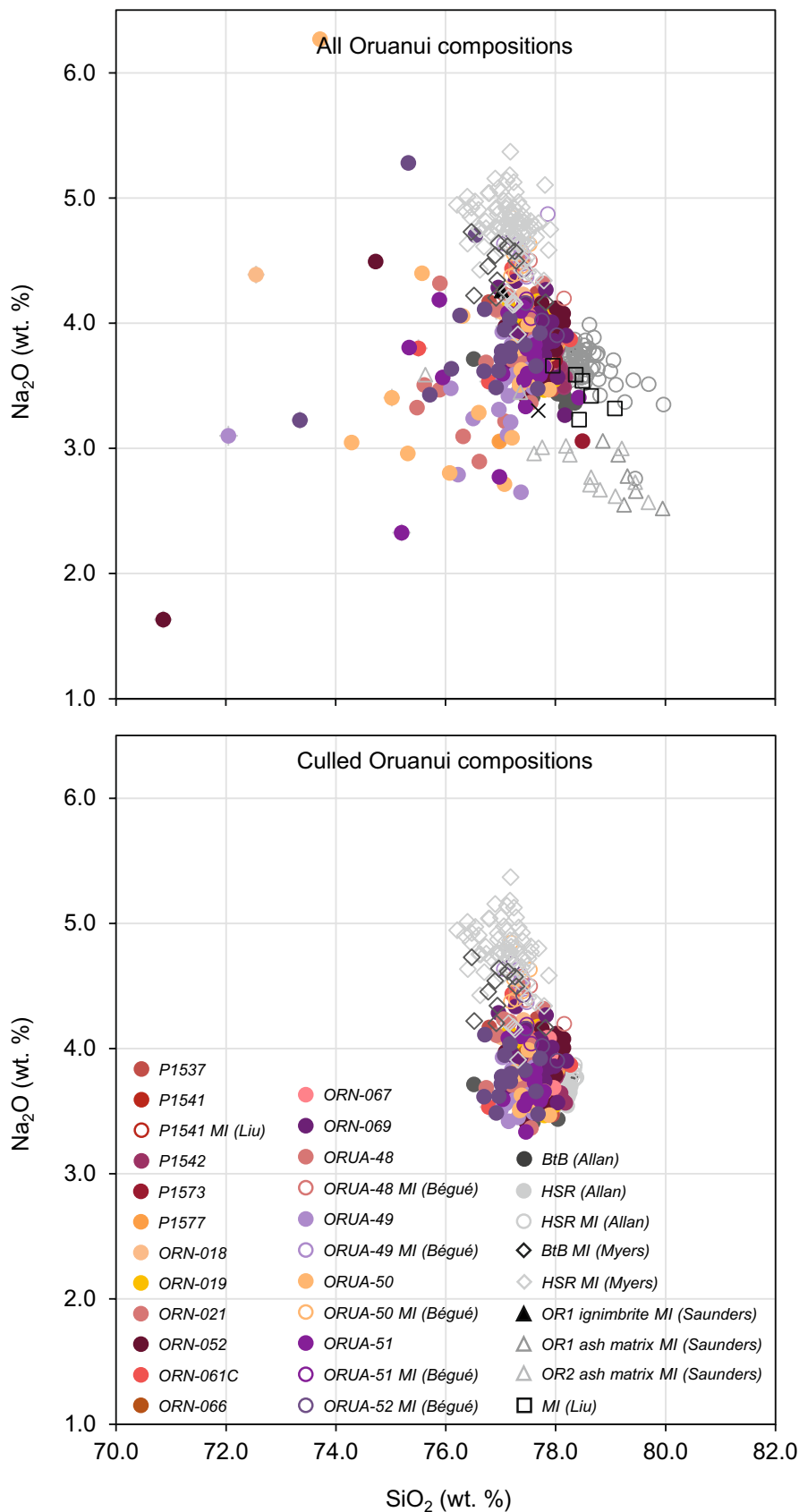
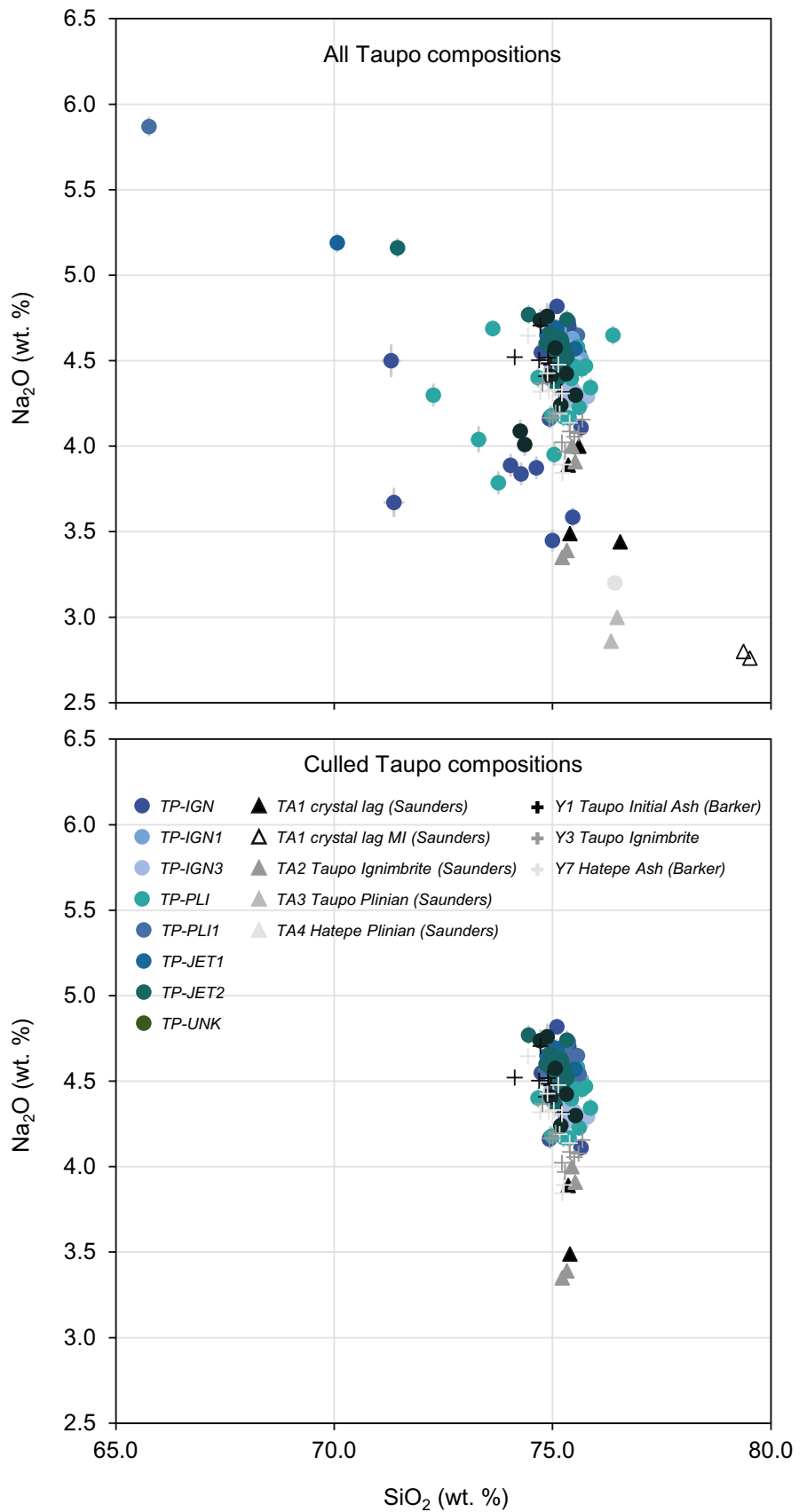


Fig. 3 SiO₂ vs. Na₂O contents of all Taupo glass compositions. Literature compositions are those with author names in parentheses. Filled symbols = Matrix glass. Open symbols = Melt inclusion (MI). (Top) All compositions that gave rhyolite-MELTS pressures. (Bottom) The final dataset after outliers were removed. Error bars on new data (filled color circles) are 2σ uncertainties; those not visible are smaller than the symbol



post-quench or post-entrapment (for melt inclusions) modification of the glass. In addition, given that the Q1F saturation condition is not as precise as Q2F (Gualda and Ghiorso 2013, 2014; Bégué et al. 2014b; Pamukcu et al. 2015a), outliers are likely to still remain in the dataset. To identify and minimize these, we compared the major element contents of glasses from successful simulations and removed clearly spurious compositions. After this winnowing process, which was done conservatively, 694 glass analyses (492 Oruanui, 201 Taupo) remained (Figs. 2, 3). The original dataset, with discarded analyses noted, can be found in the Supplementary Material 1.

Comparison of glass major element compositions from our samples reveals two general groups that correlate with the two eruptions, display no substantial overlap and are consistent with compositions published by others (Figs. 2, 3, 4, Supplementary Material 1). Our Oruanui matrix glass compositions are high-silica rhyolite (76.7–78.3 wt%) and plot with the high-silica glass analyzed by Allan et al. (2013, 2017); none are in the high K_2O /low CaO realm of the biotite-bearing lapilli (Allan et al. 2012) nor in the low-silica realm of some of the glass found by Allan et al. (2013, 2017) (Fig. 5). Taupo matrix glass is low-silica rhyolite (74.5–75.9 wt%) and overlaps in SiO_2 content with analyses published by Barker et al. (2015) and Saunders (2009); however, their analyses range to much lower Na_2O and K_2O contents (Fig. 4). Our Taupo glass is all less evolved than high-silica Oruanui glass but it does overlap with low-silica Oruanui glass (Fig. 4) identified by Allan et al. (2013). Similar to other studies (Wilson et al. 2006; Charlier et al. 2005; Allan et al. 2017; Dunbar et al. 1989a, b; Sutton et al. 1995; Barker et al. 2015), we see no relationship between composition and eruptive phase in either system (Fig. 6).

Rhyolite-MELTS geobarometry

The highly evolved nature of the Oruanui glass results in generally low crystallization pressures, relative to those from Taupo (Figs. 4, 6, 7, 8, 9), as expected from the variation in the position of the quartz-feldspar cotectic as a function of pressure (Tuttle and Bowen 1958; Johannes and Holtz 1996; Blundy and Cashman 2001; Gualda et al. 2012; Gualda and Ghiorso 2013). Our Oruanui glass compositions give pressures of 50–250 MPa, while the lower silica Taupo glass gives pressures of 280–470 MPa. Calculations run on compositions from the literature extend these ranges to 40–460 MPa (74.2–78.5 wt% SiO_2) for Oruanui and 115–470 MPa (74.1–75.9 wt% SiO_2) for Taupo. Pressure estimates for Taupo units that we did not identify quartz in are maxima; however, those from the quartz-bearing Taupo ignimbrite unit cover nearly the entire range (~270–430 MPa).

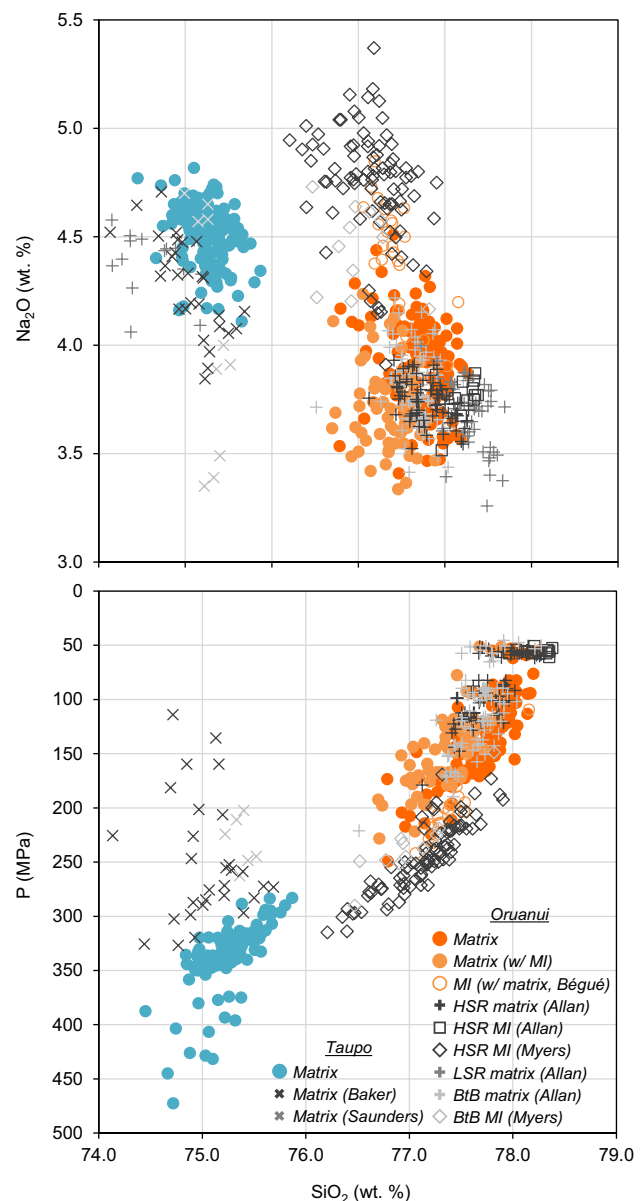


Fig. 4 Comparison of (top) SiO_2 vs. Na_2O and (bottom) SiO_2 vs. rhyolite-MELTS pressures from Oruanui (ORN) and Taupo (TP) glass compositions. Literature compositions are those with author names in parentheses

In addition to determining individual pressures from each analysis, we also estimated an average pressure for each sample. For this, we ran the rhyolite-MELTS geobarometer on an average glass composition calculated for each sample from the winnowed dataset. Pressures calculated from these average compositions range from 50 to 215 MPa in Oruanui and 290–320 MPa in Taupo (Fig. 7).

As with the compositional data, there is no relationship between eruptive phase and pressure (Figs. 6, 9). Our pressure estimates from Oruanui quartz-hosted melt inclusions are, however, higher than those we estimate for matrix glass

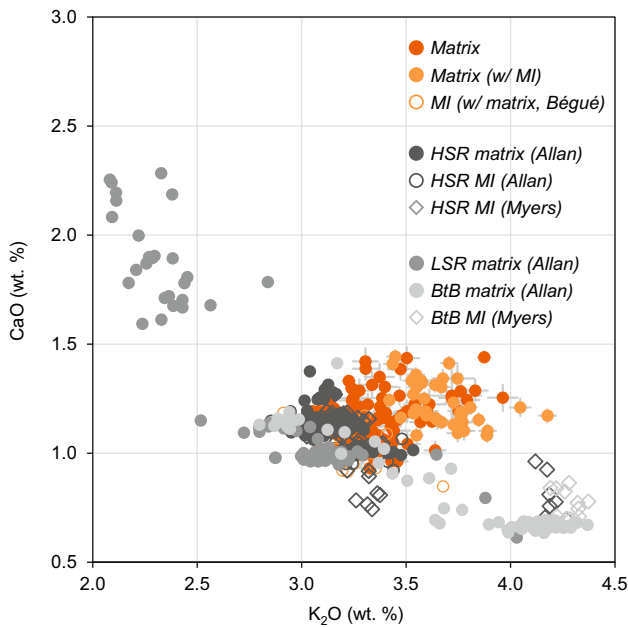


Fig. 5 Comparison of K_2O vs CaO in Oruanui samples shows that all of the glass analyses collected for this study overlap with the high-silica rhyolite (HSR) compositions found in previous studies. None of the new analyses fall into the rare low-silica rhyolite (LSR) or biotite-bearing (BtB) rhyolite categories identified previously in the Oruanui deposits. Literature compositions are those with author names in parentheses. Error bars on new data (filled color circles) are 2σ uncertainties; those not visible are smaller than the symbol

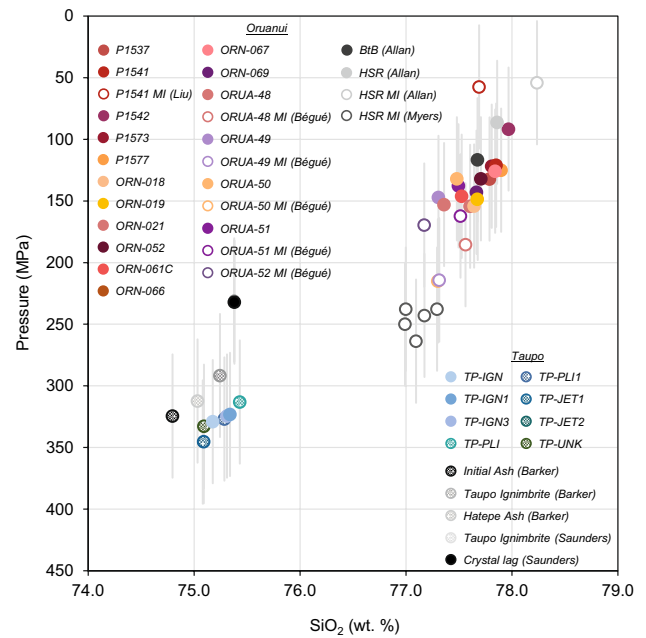


Fig. 7 Plot of SiO_2 vs. rhyolite-MELTS pressure for average Oruanui and Taupo glass compositions (see text for details). Hashed symbols indicate Taupo units where quartz has not been found. Literature compositions are those with author names in parentheses. Error bars are 2σ uncertainty (50 MPa) on rhyolite-MELTS pressure estimates

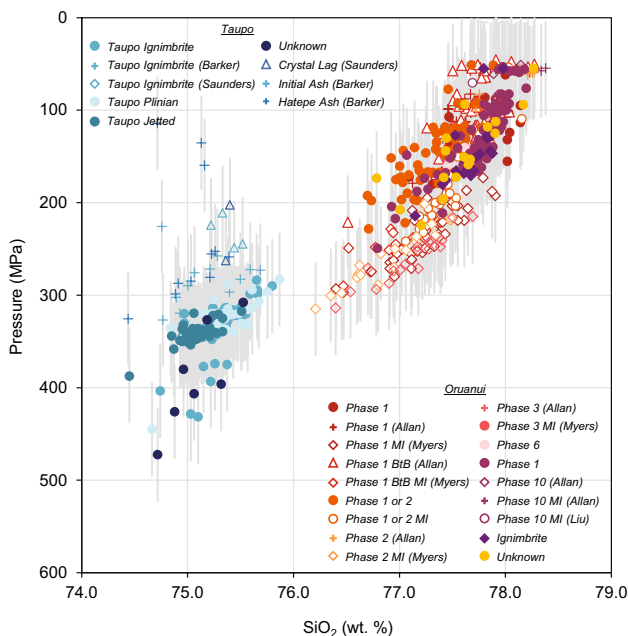


Fig. 6 Comparison of SiO_2 vs. pressure from all glass analyses used in this study delineated by eruptive unit. Literature compositions are those with author names in parentheses. Error bars are 2σ uncertainty (50 MPa) on rhyolite-MELTS pressure estimates

from the same sample (Figs. 4, 8) and are similar to those determined previously by H_2O-CO_2 geobarometry on melt inclusions from the same samples Liu et al. (2007).

Wilke et al. (2017) suggest that the rhyolite-MELTS geobarometer may underestimate pressures; however, we find that while their DERP geobarometer does give higher pressures for the same compositions, some of them are unreasonably high (> 500 MPa, outside their calibration and below the Moho for the central TVZ), and the relative differences in pressures recorded by Oruanui and Taupo glasses remain nearly the same (Fig. 10). Importantly, Gualda et al. (2019) demonstrate the DERP results are often inaccurate. Thus, regardless of the method used, glass geobarometry suggests a pronounced difference in the residence depths of these two systems.

Crystal size distributions

Plagioclase + quartz size distributions (Fig. 11) from both eruptions show decreasing population density with increasing crystal size, as is commonly observed in systems dominated by simple cooling and crystallization (Marsh 1998). Magnetite + ilmenite crystals and zircon crystals were found in every sample; however, they were not found in every tomographic scan, and the total number of crystals per sample was often well below what can

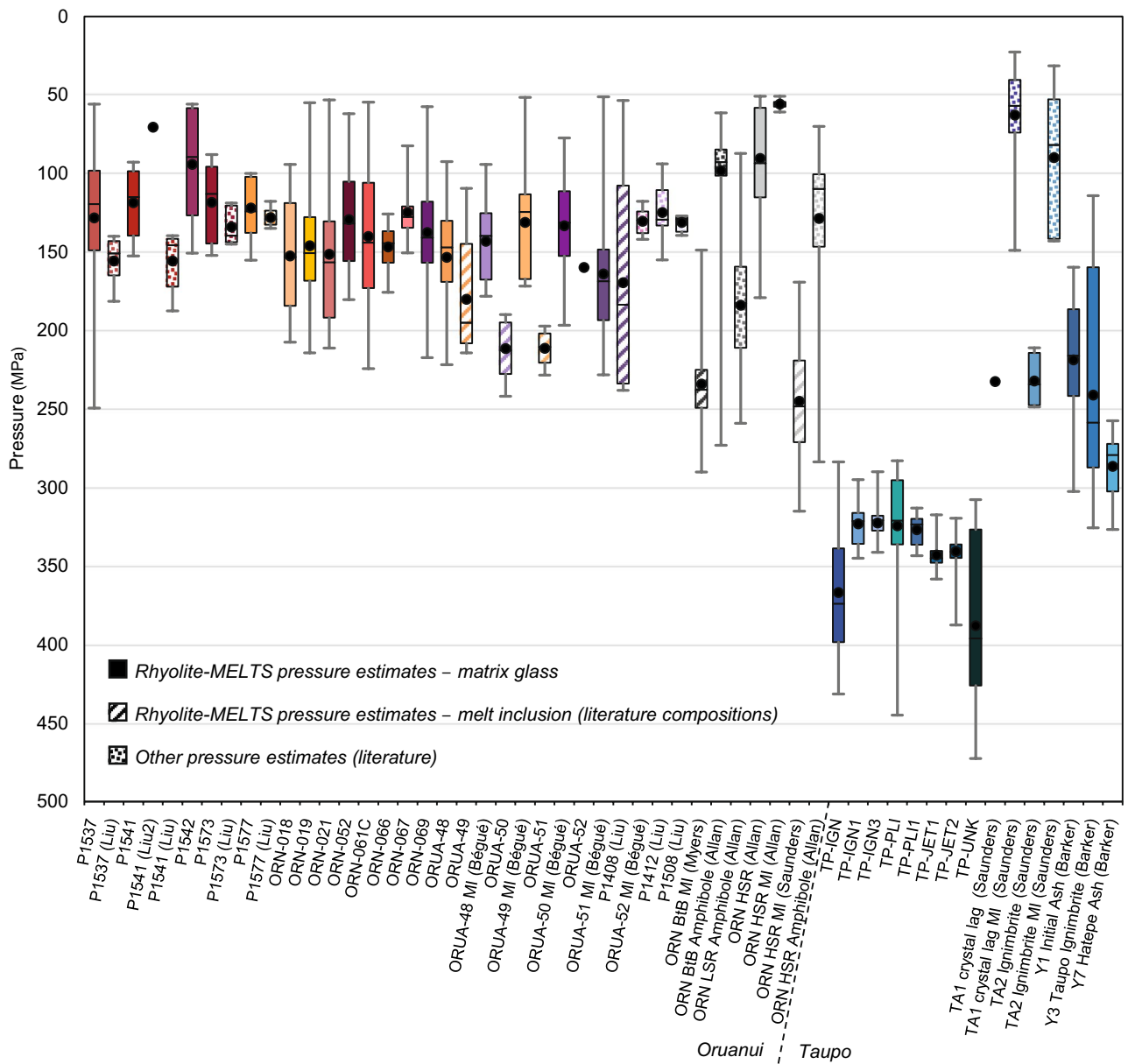


Fig. 8 Box-and-whisker plot showing pressures determined for each sample. Literature compositions are those with author names in parentheses. Pressures determined in previous studies include those

reasonably be used to construct a CSD (order 100 crystals; Gualda and Rivers 2006). Magnetite + ilmenite crystals are particularly rare and small in Oruanui samples (generally $< 300 \mu\text{m}$). They are notably more abundant and larger (up to $\sim 1340 \mu\text{m}$) in Taupo samples; two Taupo samples contained enough crystals to produce CSDs, which also show decreasing population density with increasing size (Fig. 11d). Zircon CSDs could not be constructed; crystals were rare and small (max size $\sim 200 \mu\text{m}$, with most $< 100 \mu\text{m}$) in Oruanui samples and absent in Taupo samples.

from $\text{H}_2\text{O}-\text{CO}_2$ solubility in melt inclusions (Liu et al. 2007), amphibole geobarometry (Allan et al. 2012, 2017), and orthopyroxene stabilities (Saunders 2009)

Akin to CSDs from other volcanic systems, (e.g., late-erupted Bishop Tuff, Gualda et al. 2012; Pamukcu et al. 2012; Peach Spring Tuff, Pamukcu et al. 2013; Makaopuhi Lava Lake, Cashman and Marsh 1988; Lassen Peak, Salisbury et al. 2008), Taupo CSDs are kinked, with a shallow-sloped section describing large crystals and a steep-sloped section describing small crystals (Fig. 11). Oruanui CSDs are not kinked and do not contain crystals $< 75 \mu\text{m}$ in diameter. The smallest crystals we can quantify in our highest resolution tomograms are $\sim 8 \mu\text{m}$ in size ($\sim 2 \mu\text{m}$ per voxel in each linear dimension; see Gualda and Rivers 2006), so

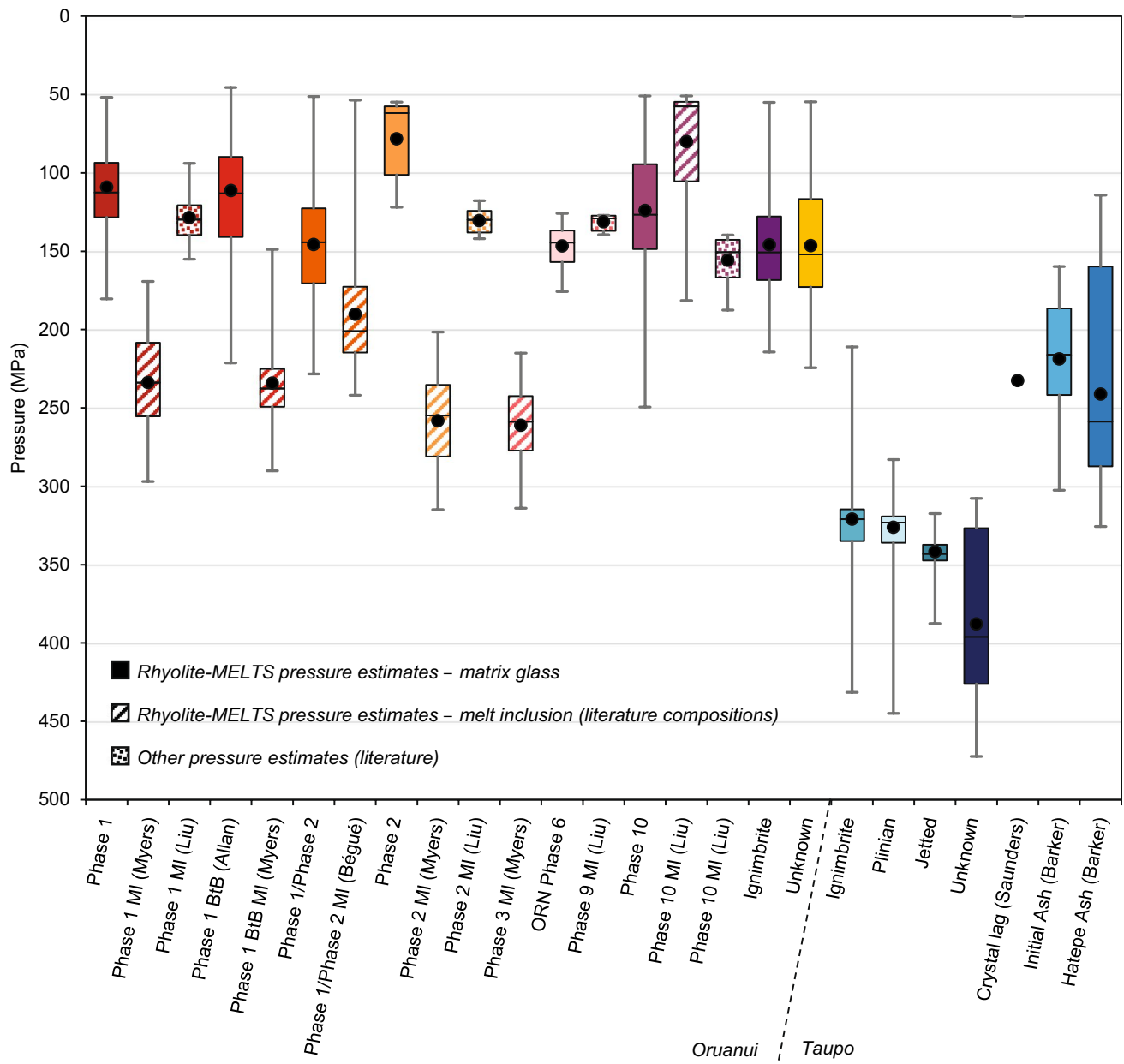


Fig. 9 Box-and-whisker plot showing pressures determined for each eruptive unit studied. Literature compositions are those with author names in parentheses. Pressures determined in previous studies are from H₂O–CO₂ solubility in melt inclusions (Liu et al. 2007)

it is possible that a small crystal population is present in the Oruanui samples but the crystals may be too small to be detected. However, efforts using BSE images of pumice chips to investigate this possibility maintains these results – no tiny crystals have yet been found.

Kinked CSDs from crystal-poor silicic magmas, where mixing of crystal populations from different magmas is not expected to define the crystal population, have been interpreted as reflecting a change in crystallization regime from growth-dominated (shallow-slope, crystallization of phenocrysts) to nucleation-dominated (steep-slope,

crystallization of groundmass; see Gualda et al. 2004; Pamukcu et al. 2012). This change is often attributed to a fundamental change in magmatic conditions. Namely, that some event, such as decompression or degassing, drives the system to favor crystal nucleation over growth (Blundy and Cashman 2005; Cashman 1992; Pamukcu et al. 2012, 2013). Consequently, we calculate slopes from each of these CSD segments independently and employ different ranges of growth rates in timescale calculations. For plagioclase + quartz, we use conservatively large ranges of 10^{-12} – 10^{-14} m/s for phenocrysts (Pamukcu et al. 2016;

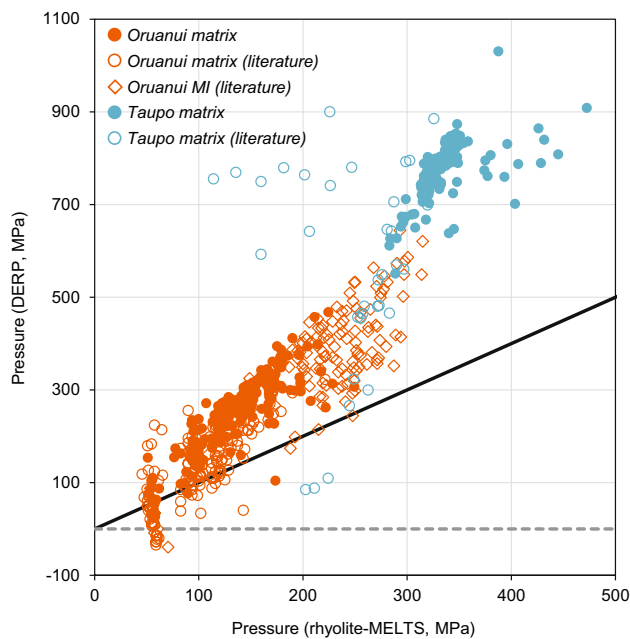


Fig. 10 Comparison of pressures from rhyolite-MELTS geobarometry and DERP geobarometry. Filled symbols are matrix glass compositions collected for this study. Open symbols are matrix glass and melt inclusion compositions from the literature. Solid line is 1:1 line

Gualda et al. 2018; this study [see “Diffusion chronometry and quartz growth rates”]) and 10^{-10} – 10^{-13} m/s for groundmass (Cashman 1988; Hammer and Rutherford 2002; Zellmer and Clavero 2006; Gualda and Sutton 2016; Befus and Andres 2018). For magnetite + ilmenite, we use rates of 10^{-14} – 10^{-15} m/s for phenocrysts (Cashman 1988) and 10^{-12} – 10^{-14} m/s for groundmass (Pamukcu et al. 2013); these growth rates are especially poorly-constrained, particularly for groundmass crystallization, so they are maxima (see Pamukcu et al. 2013).

Phenocryst segments of plagioclase + quartz size distributions from both eruptions give crystallization times ranging from decades to a few millennia (Table 2). In Taupo distributions (Fig. 11b, c), the bin where the kink occurs varies (52.5–210 μm), but the slopes of the groundmass segments are similar and give timescales of days to a few decades (Table 2). In both of the Taupo magnetite + ilmenite size distributions (Fig. 11d) the kink occurs in the 105 μm bin. Phenocryst segments of these distributions give timescales of centuries to millennia, while groundmass segments give timescales of days to a few decades (Table 2). Using the largest zircon crystals (200 μm in Oruanui samples) and an average growth rate of 3×10^{-16} m/s (Schmitt et al. 2011) gives much longer timescales (~ 21 ka) than our other CSDs. It is worth noting that there is evidence for older recycled zircon in this system (e.g., Wilson and Charlier 2009; Charlier et al. 2005) and, more generally, that zircon commonly records

much longer histories than other phenocrysts (e.g., Cooper and Kent 2014; Gualda et al. 2012; Gualda and Sutton 2016).

Diffusion chronometry and quartz growth rates

CL images of Oruanui quartz crystals reveal a variety of zoning patterns, both at the grain scale and in intricate oscillatory zoning (Supplementary Material 3), with no particular patterns dominating. For diffusion chronometry, we focus on the boundaries that show large variations in CL, because those are more clearly linked to Ti contents (e.g., Gualda et al. 2012; Pamukcu et al. 2015b; Matthews et al. 2012; Gualda and Sutton 2016; Gualda et al. 2018). These boundaries yield timescales of centuries; the maximum estimate, inclusive of our ± 30 °C temperature uncertainty, is ~ 300 a (Figs. 12, 13; Supplementary Material 2). We do not find a systematic difference between rim and interior timescales; however, smoothing of our rim profiles, due to the relatively high beam energy used in imaging (15 kV), may be significant enough to obscure any differences between zones at different positions of the crystals (i.e., we cannot reliably resolve timescales shorter than ~ 5 years at 770 °C).

Average quartz growth rates calculated from diffusion profiles (Fig. 12, Supplementary Material 2) peak at 10^{-12} – $10^{-12.5}$ m/s.; rim rates are shifted slightly slower. These values are consistent with other estimates for Oruanui quartz growth from melt inclusion faceting (10^{-12} m/s, Pamukcu et al. 2015b) and those determined for quartz in other large-volume systems (e.g., Bishop Tuff: $10^{-11.5}$ – 10^{-14} m/s, Gualda et al. 2012 and 10^{-12} m/s, Pamukcu et al. 2015b; El Quemado Complex: 10^{-12} m/s, Seitz et al. 2016; TVZ flare-up: 10^{-12} – 10^{-13} m/s, Gualda et al. 2018).

Decompression simulations

Isothermal and adiabatic decompression simulations for both systems give an overall similar result of increasing crystallization with decompression, with Taupo crystallizing substantially more than Oruanui. In both sets of simulations, crystallinity increases in ~ 1 wt% increments with 5 MPa steps in pressure, until ~ 10 wt% crystals is reached. After this point, crystallinity increases more rapidly with decompression, particularly for Oruanui; this is most pronounced in isothermal simulations. In both systems and sets of simulations, the estimated crystallinity over the entire decompression range is well above that found in natural samples (3–13 wt% in Oruanui, 1–5 wt% in Taupo); the simulations suggest that the range of crystallinity seen in the natural samples could have crystallized over a pressure range of ~ 70 MPa for Oruanui and only ~ 25 – 40 MPa for Taupo.

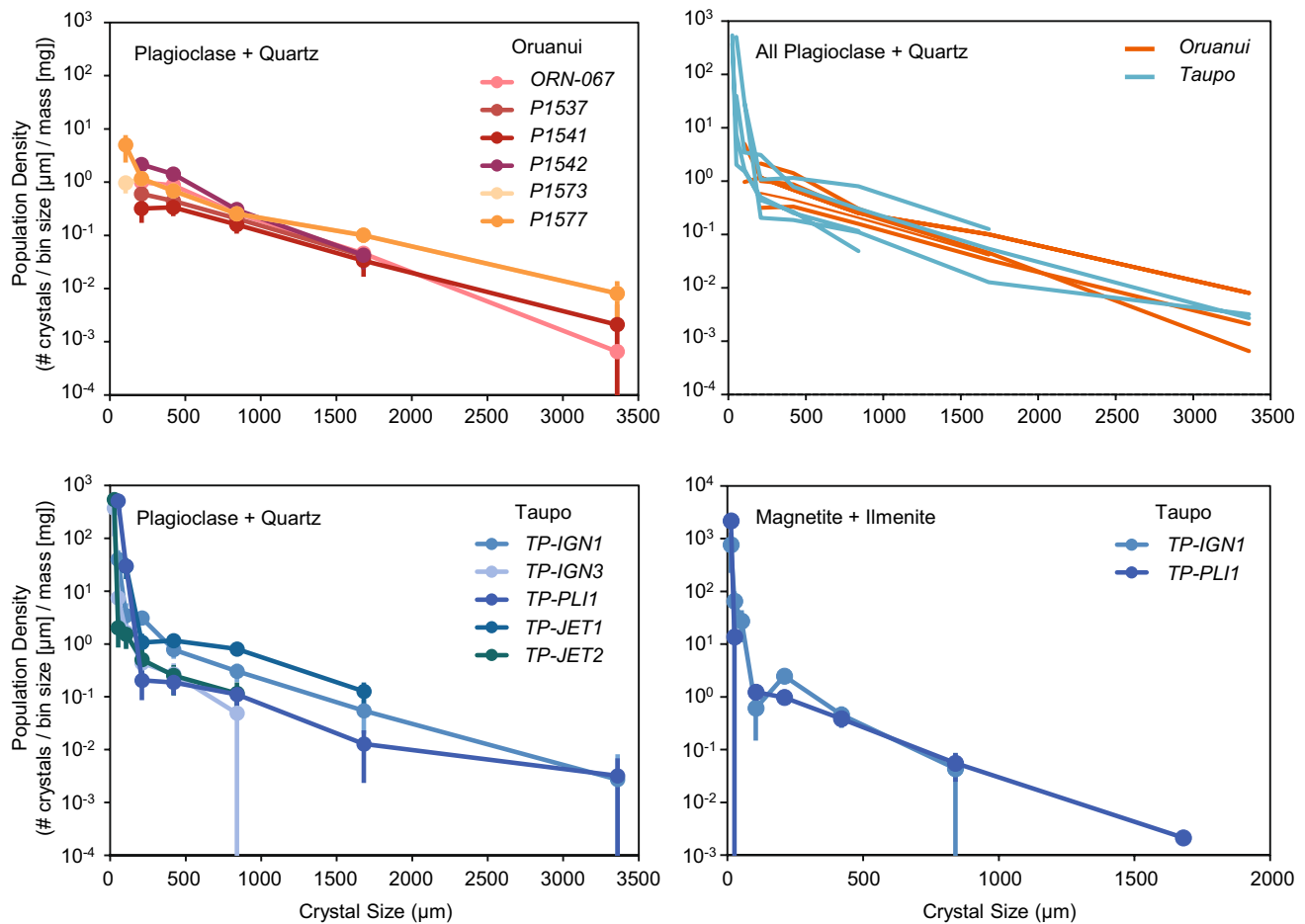


Fig. 11 a, b Plagioclase + quartz size distributions for (top) Oruanui and (bottom) Taupo samples. c Comparison of Oruanui and Taupo plagioclase + quartz size distributions. d Magnetite + ilmenite size

distributions for two Taupo samples. Other samples did not contain enough crystals to make a robust size distribution

Discussion

Melt inclusion compositions in Oruanui

Allan et al. (2017) and Liu et al. (2007) identified quartz-hosted melt inclusions in Oruanui pumice that have more evolved compositions (high Rb/Sr, low incompatible trace elements) than their host matrix glass. This is an interesting observation that has been important in arguments that the Oruanui quartz population is predominantly antecrystic or xenocrystic. Both of these interpretations have implications for interpreting timescales obtained from quartz.

In light of this, it is worth noting that nearly all of the rhyolite-MELTS simulations involving these evolved compositions failed to give pressures (Figs. 2, 14). This suggests that these compositions may be altered (Gualda and Ghiorso 2013) or that the analyses may have been affected by secondary fluorescence of the quartz host (i.e., result in anomalously high SiO₂ contents) or other analytical issues.

Given that these compositions are all significantly more silicic than the compositions that were successful, including those from quartz-hosted melt inclusions analyzed by Bégué et al. (2014b), Myers et al. (2018) and Saunders (2009), the latter issue may be the source of the errant compositions (Fig. 14). This is further supported by the fact that the successful melt inclusion compositions from Allan et al. (2017) and Liu et al. (2007) had the lowest SiO₂ concentrations of their datasets.

Magma storage at the TVC

Results of our rhyolite-MELTS analyses indicate that although the Oruanui and Taupo magmas both crystallized in the upper crust, they did so within distinct pressure ranges. Namely, we find that the Oruanui magma crystallized over a wide range of relatively shallow pressures (average ~50–215 MPa), while the Taupo magma crystallized over a much more constrained range of pressures

Table 2 Parameters for best-fit exponential curves and estimated crystallization times for plagioclase + quartz and magnetite + ilmenite crystal size distributions of pumice clasts from the Oruanui and Taupo eruptions

Phenocrysts						
Oruanui, plagioclase + quartz						
Sample	ORN-067	P1537	P1541	P1542	P1573	P1577
– 1/Gt	– 0.0024	– 0.0018	– 0.0017	– 0.0027	– 0.0015	– 0.0017
ln(n_0)	2.01	0.93	0.57	3.79	1.22	2.03
r^{2a}	1.00	1.00	0.99	0.99	0.99	0.93
Gt (μm)	423	543	601	367	663	582
t (a) ^b	13	17	19	12	21	18
t (a) ^c	1340	1722	1905	1164	2102	1844
Taupo, plagioclase + quartz						
Sample	TP-PLI	TP-JET1	TP-JET2	TP-IGN1	TP-IGN3	
– 1/Gt	– 0.0014	– 0.0015	– 0.0025	– 0.0035	– 0.0022	
ln(n_0)	0.28	1.99	6.55	1.70	2.92	
r^{2a}	0.95	0.92	0.66	0.88	0.97	
Gt (μm)	710	651	402	284	462	
t (a) ^b	22	21	13	9	15	
t (a) ^c	2249	2063	1275	900	1465	
Microlites						
Taupo, plagioclase + quartz			Taupo, magnetite + ilmenite			
Sample	TP-PLI	TP-IGN1	Sample	TP-PLI	TP-IGN1	
– 1/Gt	– 0.3927	– 0.0711	– 1/Gt	– 0.3860	– 0.0611	
ln(n_0)	409,227.1	995.1	ln(n_0)	343,864.4	432.8	
r^{2a}	1.00	0.95	r^{2a}	1.00	0.97	
Gt (μm)	3	14	Gt (μm)	3	16	
t (h) ^d	7.074	39.075	t (a) ^b	0.08	1	
t (d) ^b	29	163	t (a) ^c	8	52	

^aCoefficient of determination (1: perfect correlation)

^bGrowth rate used: 10^{-12} m/s (see text for details)

^cGrowth rate used: 10^{-14} m/s (see text for details)

^dGrowth rate used: 10^{-10} m/s (see text for details)

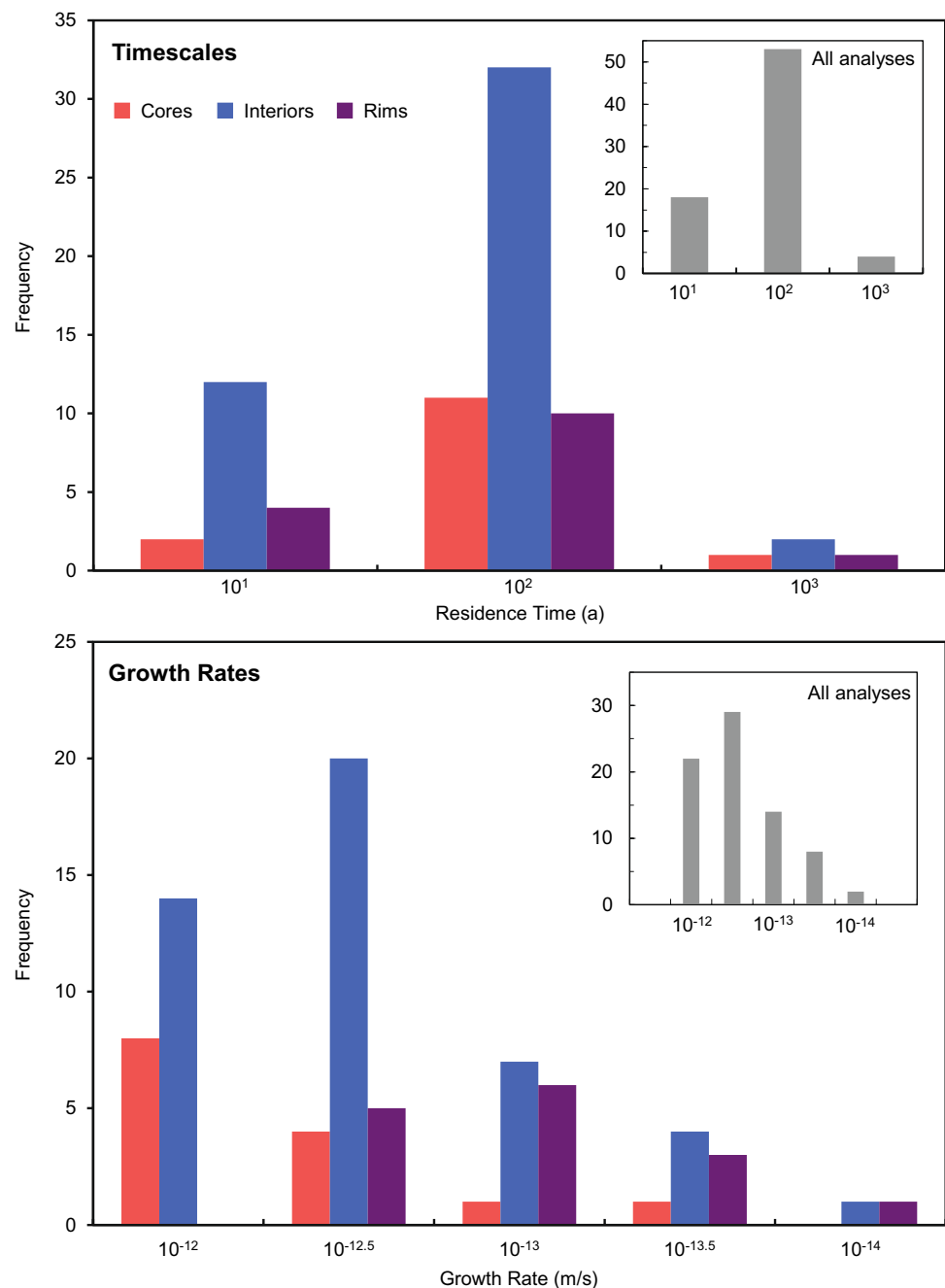
significantly deeper in the crust (average ~290–350 MPa). This is particularly well-illustrated in the pressure estimates from average glass compositions (Fig. 7), but it is also evident in the estimates determined from individual analyses (Figs. 4, 6).

The consistency in the results from Taupo is especially noteworthy given that quartz is rare in these samples. Pressures from those units that do not contain quartz are technically maxima; however, the fact that they overlap with pressures from units that did contain quartz (Fig. 7) suggests that they are likely appropriate estimates of crystallization pressures. Notably, the low crystal contents of Taupo samples may make finding quartz challenging, and it is interesting that Saunders (2009) reported finding quartz only in the most crystal-rich samples (2–5 wt% crystals) and Houghton

et al. (2012), who studied hundreds of samples with 2–3.5 wt% crystals, also found quartz in the Taupo phenocryst assemblage—this is consistent with our own observations, and it suggests that melts generally equilibrated with quartz in the Taupo system.

Our pressures are broadly consistent with previous estimates for the Oruanui system, but they are substantially higher than most of those determined for Taupo. This is noteworthy in light of past work exploring silicic volcanism at both Taupo volcano in particular and in the central TVZ more generally. First, multiple studies suggest that the Taupo magma did not exist in the crust at the time of the Oruanui eruption and that the magmatic system at the TVC was obliterated and entirely rebuilt after the supereruption (Sutton et al. 1995, 2000; Smith et al. 2005; Gelman et al.

Fig. 12 Comparison of (top) timescales and (bottom) growth rates from Ti-in-quartz diffusion chronometry of cores, interiors, and rim zones in Oruanui quartz crystals. Insets show results from all analyses amalgamated



2013; Barker et al. 2014, 2015). In particular, Gelman et al. (2013) demonstrated that the first erupted magma following the Oruanui caldera-forming event, the Omega dacite, represents a deeper magma recharge from a new source and kicked off the reconstruction of the TVC. Further, Barker et al. (2015) propose that: (a) the post-Oruanui mush system spatially overlapped the original Oruanui system, (b) the post-Oruanui rhyolites, including the Taupo magma, were derived from a single magmatic system, with changing crystallization conditions through time, and (c) the post-Oruanui rhyolites crystallized at similarly shallow depths

as the Oruanui magma (~5–8 km). Our results for Taupo are not wholly consistent with this model, as our pressure data suggest the Taupo magma resided at deeper pressures (~10–16 km) more similar to those estimated for the original Oruanui source mush (~6–12 km; Allan et al. 2013, 2017). This suggests three possibilities: (1) the post-Oruanui magmatic system was not as vertically extensive (to low pressures) as the Oruanui system, (2) the Taupo magmatic system was distinct from Oruanui and other post-Oruanui systems, or (3) the Taupo magma was extracted from a deep mush and immediately erupted, with no period of shallow

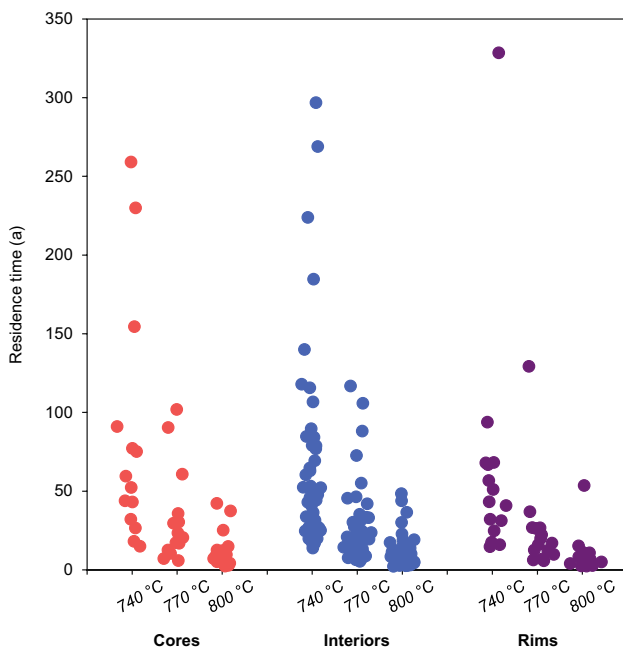


Fig. 13 Timescales from Ti-in-quartz diffusion chronometry as a function of temperature. A temperature uncertainty of ± 30 °C was used in diffusion modeling. Note that results differ by less than an order of magnitude

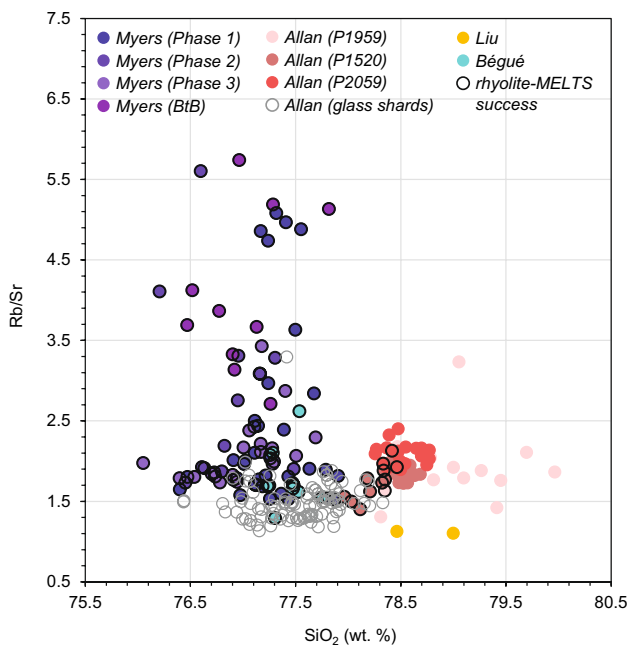


Fig. 14 SiO₂ vs. Rb/Sr contents of published melt inclusion compositions. Rhyolite-MELTS geobarometry simulations of compositions without a black outline failed

storage before the eruption. Interestingly, Sutton et al. (1995, 2000) and Smith et al. (2005) suggest that the SG2 and SG3 rhyolites, including Taupo, did come from magmatic systems, depths, and sources distinct from preceding rhyolites; however, Barker et al. (2015) attribute the compositional changes used in their arguments to changes in crystallization conditions, rather than a change in the magmatic system and source.

Second, our data illustrate the most recent distribution of extensive volumes of silicic magma in the crust at the TVC, and it is interesting to compare this with previous periods of large-volume silicic magmatism in the central TVZ. In particular, Gualda et al. (2018) assessed the evolution of storage depths in the central TVZ during the < 100 ka ignimbrite ‘flare-up’ (~350–280 ka; Gravley et al. 2016), during which eight caldera-forming eruptions occurred. They estimated shallow pressures for the magmas erupted in phase 1 of the flare up (the much larger Whakamaru Group ignimbrites supereruption, > 2000 km³, ≤ 100 MPa), followed by a significant deepening of magma storage at the beginning of phase 2 (Chimpanzee, 50 km³, ~150–250 MPa), when the post-Whakamaru magma system reconstruction was starting on the western side of the central TVZ. As this new system matured, they found a progressive shallowing of storage depths (from a dominant peak at ~150 to ≤ 100 MPa) and increasing eruption size (up to ~250 km³ for the culminating paired Ohakuri and Mamaku eruptions) through the remainder of the flare-up.

In comparison, our storage pressure estimates for the recent TVC show a marked shift from shallow (Oruanui) to deep (Taupo); Barker et al. (2015) also found this to be the case for eruptions through the post-Oruanui SG1 period. Thus, we see a similar transition as Gualda et al. (2018) did, from shallow storage of a giant, mature magma to deep storage of a large, less mature magma during the reconstruction of the TVC system. At the TVC, this transition occurred over ~24 ka, which is also a similar timescale to the ~20–40 ka suggested between the end of phase 1 and start of phase 2 in the flare up (Gravley et al. 2016).

In the case of the ‘flare-up’ magmas, Gualda et al. (2018) hypothesized that the shallowing of magma storage was the result of an interplay between tectonics—external forcing due to crustal extension—and magmatism—internal forcing due to heat transfer and conditioning of the crust by preceding magmatic intrusions. At the TVC, similar forcings were at play: up to 26 other eruptions at the volcanic center preceded the formation of the eruptible Taupo magma body (internal forcing), and this post-Oruanui activity was potentially induced by rifting (external forcing; see Barker et al. 2015, 2016). Consequently, the storage depth pattern that we find for the recent TVC may suggest that this magmatic center is in the midst of a new cycle of large caldera-forming eruption events. Notably,

given the eruption and mantle input rates suggested by the caldera-forming magmatic activity in the central TVZ over the past ~ 60 ka, and possibly related to a partial melt anomaly in the mantle directly beneath the central part of the TVZ (Eberhart-Phillips et al. 2008), Gravley et al. (2016) also propose that the modern TVZ may be flaring up. Alternatively, or more generally, we may be identifying a pattern that most mature systems in the TVZ crust are shallow and vertically extensive (like the flare-up Ohakuri-Mamaku magmas), while those in less mature, reconstructing systems are smaller and deeper. This is not necessarily surprising, however, as the higher silica contents of the more mature systems are consistent with their storage at shallower pressures (Gualda and Ghiorso 2013).

Finally, considering Oruanui alone, the wide span of pressures that we estimate for this system has implications for understanding its geometry in the crust. Previous studies suggest the Oruanui deposit represents the eruption of a single giant volume of crystal-poor magma (Allan et al. 2017; Wilson et al. 2006), and the lack of distinct pressure regimes in our geobarometry results certainly makes this a possible interpretation of our data. It is interesting to note, however, that we find two broad pressure populations amongst our high-silica glass compositions—one falls coherently over a wide range from ~ 80 to 250 MPa, while another population is distinct at ~ 50 MPa (Figs. 4, 6). Matrix melt can evolve in composition with time, so it is possible, even likely, that these are not the starting crystallization depths of these magmas. In fact, in cases where we have matching matrix glass and melt inclusion data, we find that the matrix glass is more evolved and gives equal-to-lower pressures (Figs. 7, 8) (see Gualda and Ghiorso 2013). This suggests that, in some cases, the melt (now matrix) did indeed evolve after melt inclusion entrapment. Nonetheless, the existence of these two populations may indicate that there were two magma batches at distinct starting depths.

While we cannot conclusively discern if a multiple magma batch model is appropriate, it is not impossible for the TVZ: Allan et al. (2013) identified biotite-bearing lapilli in Oruanui deposits that they suggest derived from a magma batch that migrated laterally and mixed with the Oruanui magma during the eruption; Gravley et al. (2007) and Bégué et al. (2014a) proposed that multiple magma batches were involved in the paired Mamaku and Ohakuri eruption in the central TVZ; Cooper et al. (2012) identified different glass compositions in the Kidnappers supereruption and suggested three independent magma bodies were systematically tapped during the eruption; and Heise et al. (2007) have identified multiple low-resistivity zones in the TVC crust today, which may be evidence of multiple melt batches. Alternatively, as we discuss below, the pressure groups we see in the Oruanui data may be evidence for stepped decompression of the Oruanui system.

Crystallization timescales

Crystals are the primary repository of time information in volcanic deposits, and efforts to develop, employ, and establish a framework for comparing timescales from different crystal-based geochronometers, particularly for large-volume silicic systems, highlight the extensive lifetime of these systems (e.g., Cooper and Kent 2012; Gualda and Sutton 2016): from the thermal priming of the crust and building of a source mush (10^4 – 10^6 a), to the extraction and pre-eruptive crystallization of the eruptible crystal-poor magma (10^1 – 10^3 a), to syn-eruptive degassing and decompression (≤ 1 a). Here, we use time records contained in different portions of the crystal population—phenocrysts and microlites—and different mineral phases to investigate the timing and duration of two of these stages in the Oruanui and Taupo magmatic systems: the pre-eruptive residence of the eruptible, melt-rich magma bodies, and the syn-eruptive process of magma ascent and decompression. We use two independent methods—CSDs and Ti diffusion chronometry in quartz—and we capitalize on the high time-resolution (< 1 – 10^4 a) achievable with such geochronometry methods to investigate the shorter timescales associated with these stages.

Phenocrysts are large and can record an extensive history of crystallization, while the tiny size of microlites, which comprise the groundmass of many volcanic rocks, suggests these crystals grew near to the time of eruption or during the eruptive process. Consequently, we use timescales from phenocrysts—recorded in both the shallow-sloped sections of CSDs describing large crystals and diffusion profiles across zone boundaries in the cores and interiors of crystals—to study pre-eruptive magma residence (following Pamukcu et al. 2012; Gualda et al. 2012). We use timescales from microlites—recorded in the steep-sloped sections of CSDs describing small crystals—to investigate syn-eruptive processes (Pamukcu et al. 2012). In some cases, diffusion profiles across zone boundaries on the rims of phenocrysts may also provide information on these latter timescales (Gualda and Sutton 2016; Pamukcu et al. 2016).

Importantly, we recognize and try to mitigate the limitations of these methods. Recent work suggests that magmatic systems may incur protracted and/or multiple periods in a state of lock-up, when the magma is crystal-rich, relatively cold, and uneruptible (e.g., Cooper and Kent 2012; Cashman and Blundy 2013; Rubin et al. 2017; Szymanowski et al. 2017). Unlike absolute age-dating methods based on radioactive decay, the diffusion-based nature of our geochronometers precludes us from investigating time spent in cold storage (i.e., under sluggish diffusion conditions). Consequently, we focus on the relative timing and duration of the last pre-eruptive stage of crystallization of these systems, when the final eruptible, crystal-poor magmas resided in the crust. Importantly, however, our timescale estimates for

this period are maxima: although time is not recorded during cold storage, these geochronometers accrue time whenever the system is at magmatic temperatures. Thus, the resultant time estimates are, at worst, an overestimate (some time spent subsolidus and/or the crystal population is predominantly comprised of xenocrysts) for the longevity of the final bodies of magma that fed these eruptions. In turn, if the system spent little-to-no time near or below the solidus and the crystal population is predominantly comprised of phenocrysts that grew in the final pre-eruptive magma bodies, our time estimates should be akin to the duration of the last period of pre-eruptive crystallization.

Second, different minerals saturate and crystallize under different conditions, such that they may not all record the same history. For example, rhyolite-MELTS simulations indicate that plagioclase saturated earlier than quartz in the melt-rich Oruanui high-silica rhyolite magma (Pamukcu et al. 2015b) such that quartz crystallization timescales represent only 30% of the total crystallization history, while those from plagioclase represent 100% of it. Consequently, using a single phase to assess residence times could result in underestimates. To lessen this issue, we (a) consider time records from multiple phases and (b) account for the time prior to quartz saturation; including these considerations in our interpretations does not, however, change our conclusions (e.g., the difference in time between quartz and plagioclase saturation in Oruanui is less than an order of magnitude).

Pre-eruptive crystallization and residence of the Oruanui and Taupo eruptible magmas

The parallelism of the phenocryst segments of our CSDs (Fig. 11) indicates that the Oruanui and Taupo magmas crystallized over similar timescales. Timescales calculated from the slopes of plagioclase + quartz CSDs are consistent with this and suggest a short residence of the eruptible magma bodies in the crust, on the order of decades to, at most, a few millennia (~10 a–2.3 ka; Table 2); times determined from quartz diffusion chronometry at core and interior zone boundaries of Oruanui quartz are similar (~1.5–120 a). Magnetite + ilmenite CSDs from Taupo samples record considerably longer timescales (up to 6 ka; Table 2), but the growth rates for these phases are poorly constrained maxima.

These results corroborate those from other studies. For Oruanui, residence times inferred from orthopyroxene diffusion chronometry (~18 a–1.3 ka; Allan et al. 2017), shape maturation of quartz-hosted melt inclusions (100 s of a for quartz crystallization; Pamukcu et al. 2016), and U–Th zircon model ages (<3 ka; Wilson and Charlier 2009) all suggest timescales on the order of years to a few millennia. The longevity of the Taupo magma is less well studied, but previous work using geochemical trends and thermal

modeling also suggest short residence times (0.01–1 ka; Sutton et al. 2000; Barker et al. 2015, 2016). More broadly, our calculated residence times for these magmas are similar to those determined for a number of other large-volume silicic systems (e.g., Bishop Tuff, Gualda et al. 2010; Peach Spring Tuff, Pamukcu et al. 2013; El Quemado Complex, Seitz et al. 2016; Santorini, Druitt et al. 2012; TVZ ignimbrite ‘flare-up’ eruptions, Gualda et al. 2018). This consistency suggests a greater universality of short pre-eruptive crystallization times, especially given the variety of methods used and mineral phases investigated. In other words, decadal-to-millennial residence times may be characteristic of large-to-giant volume silicic systems in general.

The similarity in our residence times for the two TVC systems is also striking because of their notable difference in volume (but similar crustal context). The volume of magma evacuated in the Oruanui eruption eclipsed that of the Taupo eruption by an order of magnitude. Consequently, our results suggest that the size of an eruption is not a function of the time over which a large-to-giant crystal-poor magma body resides in the crust in an eruptible state. Rather, we suggest that the volume of the underlying mush and/or the efficiency of melt extraction from a mush likely has a bigger impact on controlling eruption volume. Alternatively, recent work suggests that the large volumes evacuated in supereruptions may actually represent the contemporaneous eruption of multiple smaller volumes (e.g., Cooper et al. 2012; Gualda and Ghiorso 2013; Bégué et al. 2014a), which may or may not have been mixed prior to eruption. In this case, we do not necessarily expect crystallization timescales to be positively correlated with eruption volume: given that the individual magma batches involved in the eruption will have smaller volumes than the final erupted volume, the similarity in timescales that we find may just reflect crystallization of multiple, independent, similar-sized magma batches that eventually interact during the eruption. We are not able to conclusively distinguish between these scenarios, but our data do allow the possibility that the Oruanui eruption involved multiple magma batches (see previous section).

Syn-eruptive crystallization and decompression of the Oruanui and Taupo magmas

All Taupo CSDs have a kinked shape and show a significant microlite population (Fig. 11). Like other studies (e.g., Cashman 1992, Pamukcu et al. 2012), we interpret this to reflect a change in crystallization regime, from growth-dominated to nucleation-dominated, due to decompression and degassing associated with the eruption. Slopes of the CSD segments describing small crystals (microlites) are similarly steep for all samples and give short timescales, indicating that the final Taupo eruption occurred quite rapidly—within days to a few years—after the onset of the eruptive process.

Timescales from plagioclase + quartz are particularly short (7 h–163 days), while those from magnetite + ilmenite range to significantly longer times (30 days–52 a); however, this discrepancy may be due to the fact that the growth rates we use for the latter calculations are especially poorly constrained and maxima (see Pamukcu et al. 2013).

Interestingly, Oruanui samples do not exhibit these features—CSDs are notably uninked and devoid of crystals smaller than 75 μm (Fig. 11, Table 2). In addition, timescales and growth rates calculated from diffusion chronometry on rim boundaries are not especially shorter or faster, respectively, than those from core or interior zone boundaries (Fig. 12, Supplementary Material 2); in fact, rim growth rates are shifted to slower rates. This is distinct from other systems, such as the Bishop Tuff, where a record of decompression-induced fast crystal growth has been identified in quartz phenocrysts by diffusion chronometry: high-Ti/bright-CL rims of quartz crystals give extremely short timescales (minute to days) and growth rates that are many orders of magnitude faster than those from core or interior zone boundaries (Gualda and Sutton 2016). Although the resolution on our timescale calculations is limited by smoothing from the high beam energy we used for our imaging, the rim zones of Oruanui crystals are also not particularly enriched in Ti/bright in CL (Supplementary Material 3).

These textural differences suggest a substantive difference in the eruptive process for the Oruanui and Taupo systems. We consider four potential explanations for this disparity:

Differences in ascent time Results from rhyolite-MELTS geobarometry, which include data from some of the same samples we used for our textural analyses, suggest that the magma involved in the Oruanui eruption crystallized at much shallower depths than did the Taupo magma (Figs. 4, 6, 7, 8, 9). As a result, assuming the simplest scenario of an equal and constant decompression rate and linear path to the surface for both systems, the traverse to the surface during the eruption would have been shorter for the Oruanui magma than the Taupo magma. As a consequence, the time available for decompression-induced crystallization simply would have been less for Oruanui than Taupo, and we would expect our microlite crystallization times, at a given growth rate, to be shorter for Oruanui than Taupo. Furthermore, for a difference in ascent time to explain our textural results, that difference must be longer than the time needed to grow a resolvable microlite or phenocryst rim zone (10 μm in our images), given that Taupo samples contain a microlite population but Oruanui samples do not. Using average growth rates for quartz, feldspar, and Fe–Ti oxide groundmass crystallization (10^{-10} – 10^{-13} m/s; Cashman 1988, Pamukcu et al. 2012), we estimate that ~3 h–115 days are needed to grow such a resolvable microlite crystal phenocryst zone. Relevant experiments constrain this still further, suggesting

that that microlite growth is limited if decompression occurs over a period shorter than 3–8 h (Castro and Dingwell 2009; Andrews and Gardner 2010).

In fact, our microlite crystallization times do fit these constraints: they are shorter for Oruanui than Taupo—Oruanui CSDs suggest very little to no time (no microlite population), while Taupo plagioclase + quartz CSDs suggest average timescales of ~30 min (10^{-10} m/s) to ~200 days (10^{-12} m/s)—which are within the range of times we calculate are needed to grow a resolvable microlite crystal or phenocryst zone and the timescales suggested by experiments for microlite growth. Magnetite + ilmenite CSDs suggest timescales of ~30 days (10^{-12} m/s) to 5 years (10^{-13} m/s); however, as noted, growth rates for these phases are poorly constrained maxima. This suggests that differences in ascent time due to differences in the residence depths of the Oruanui and Taupo magmas could explain our textural observations.

Of course, decompression rates are not necessarily the same for both systems, and we can bring our data together with estimated decompression rates to better calculate the difference in ascent times. Liu et al. (2007) and Myers et al. (2018) determined decompression rates of ~0.001–0.01 MPa/s for the Oruanui from re-entrant melt inclusions and using these rates we calculate ascent times of ~1 h to ~3 days from our estimated storage depths. On the short end of this range, these timescales are shorter than those needed to grow a resolvable microlite or phenocryst growth zone at growth rates of 10^{-9} m/s or slower. For the longer ascent times, growth rates of 10^{-11} m/s or slower are needed. These rates are similar to those suggested by Cashman and Marsh (1988) for feldspar microlite crystallization in Mount St. Helens samples (10^{-10} – 10^{-12} m/s) but slower than those suggested by Gualda and Sutton (2016) for growth of Ti-enriched rims on Bishop Tuff quartz grains (average 10^{-8} m/s). Consequently, while the uncertainty on decompression and growth rates precludes a conclusive answer, a difference in ascent time is a potential explanation for our textural observations.

Differences in decompression rate Supersaturation is required to drive nucleation and crystal growth, but kinetic constraints can introduce a lag into these processes. Consequently, the interplay between decompression rates and kinetics can dictate crystallization regimes (Cashman and Blundy 2000). Here, we consider the implications of fast and slow decompression rates in the context of the TVC textures.

Fast decompression Textures and experiments suggest that decompression and eruption can happen too quickly for kinetics to keep pace, and these conditions will inhibit crystallization (Cashman and Blundy 2000). For example, Couch et al. (2003) found this to be the case at

Montserrat—Soufrière Hills andesites lack microlites, and from their experiments they conclude that fast decompression (> 0.009 MPa/s) was the cause. Direct comparison with the TVC systems is challenging because the composition is also related to supersaturation conditions and crystallization kinetics; however, the decompression rates estimated for the Oruanui eruption (Liu et al. 2007; Myers et al. 2018) are similar to or much faster than those determined by Couch et al. (2003).

An alternate useful comparison is with the Bishop Tuff, because the storage depths calculated for both the early- and late-erupted Bishop Tuff are similar to those for Oruanui (~175–200 MPa; Gualda and Ghiorso 2013), but both units contain quartz with Ti-enriched rims (Gualda and Sutton 2016) and a feldspar + quartz microlite population (Pamukcu and Gualda 2010); some CSDs of the early-erupted Bishop Tuff do not show a microlite population, but this could be a function of low image resolution (Gualda and Rivers 2006; Gualda et al. 2004). Myers et al. (2018) estimated decompression rates for both the early- and late-erupted Bishop Tuff, and they are similar to or faster (early-erupted: 0.0084–0.01 MPa/s; late-erupted: 0.006–0.22 MPa/s) than those they estimated for the Oruanui (0.001–0.01 MPa/s). We do not have a comparable estimate for Taupo; however, the fact that the Bishop Tuff shows evidence of decompression crystallization but similar-to-faster decompression rates than Oruanui suggests that fast decompression (i.e., > 0.001 MPa/s) cannot effectively explain the TVC discrepancy.

Slow decompression Alternatively, perhaps the decompression of Oruanui was slow such that the system never achieved the undercooling required to enhance nucleation and growth rates. Decompression rate estimates from Myers et al. (2018) do support this as those for early Oruanui eruptive phases (1 and 2; 0.026–0.034 MPa/s, average: 0.011 MPa/s) are slower than those for both the Bishop Tuff (0.006–0.22 MPa/s, average: 0.050 MPa/s) and the Huckleberry Ridge (0.007–0.064 MPa/s, average: 0.023 MPa/s) eruptions. In addition, and again, the Bishop Tuff does show textural evidence of decompression (Gualda and Sutton 2016; Pamukcu et al. 2016). Consequently, while the comparison between Oruanui and Bishop Tuff decompression rate estimates and textures suggests it is not fast decompression that hindered Oruanui microlite growth, it does not rule out the possibility that slow decompression rates in the Oruanui could be the cause.

Interestingly, Myers et al. (2018) did estimate significantly faster rates (0.012–0.016 MPa/s, average: 0.014 MPa/s) for phase 3 of the Oruanui eruption, and those rates overlap with the faster Bishop Tuff and Huckleberry Ridge rates. While none of the samples we used for our textural analyses are from phase 3, we do have data for phase 10 samples, and they also lack microlites

and Ti-enriched quartz rims. This suggests that either: (a) slow decompression is not the cause of the lack of microlites, (b) decompression rates slowed down again over the course of the eruption, or (c) there are issues with the decompression rate estimates. Notably, Liu et al. (2007) did estimate slower decompression rates for phase 10 samples, but Myers et al. (2018) suggest this may be an artifact of the older CO_2 diffusivities Liu et al. (2007) used in their models.

Differences in decompression style Several studies suggest that decompression style (e.g., continuous vs. stepped decompression), rather than decompression rate, is what ultimately dictates microlite textures (e.g., Bruegger and Hammer 2010; Hammer et al. 1999; Cashman and Blundy 2000). More specifically, they suggest that decompression followed by shallow arrest results in extensive groundmass crystallization. In light of this, it is worth considering the effect of storage depth on the ability for a magma to stall during ascent: holding all else equal, the deeper a magma resides, the longer its traverse to the surface, the more opportunity it has to stall during ascent. Following this logic, the shallowness of Oruanui would have limited the opportunities for stalling, whereas the depth of the Taupo system would provide it with more stalling potential. This would be consistent with our textural observations.

Interestingly, Myers et al. (2018) estimated pressures from both fully-enclosed and re-entrant Oruanui quartz-hosted melt inclusions and found that the fully-enclosed inclusions gave higher pressures than the innermost portion of the re-entrants. They interpret this to indicate stepped decompression of the Oruanui magma. The paucity of Oruanui microlites is not in accord with this interpretation, as stepped decompression should have facilitated the growth of microlites and crystal rims; however, a short duration of repose early in the decompression history, when crystallization on existing phenocrysts could have been sufficient, and/or slow initial ascent could have also acted concurrently to inhibit microlite crystallization.

Differences in liquidus temperatures due to differences in residence depths Liquidus temperatures of water-saturated magmas are inversely related to depth, such that the temperature is lower at higher pressures and isothermal or adiabatic decompression or degassing will drive them higher. This will increase the undercooling of a system, driving faster crystal growth and augmenting nucleation. In other words, initially deeper systems should crystallize more with decompression and degassing. Models by Hort (1998) suggest that systems can rapidly return to an equilibrium state after such perturbations, but doing so requires up to a 10% increase in crystal fraction by nucleation and crystallization. In the case of an erupting system, there is

likely not enough time between such an event and the final eruption for this relaxation to happen.

In light of this, the difference in the Oruanui and Taupo storage depths indicated by our geobarometry results allows for the possibility that the disparity in microlite textures is due to differences in the liquidus temperatures for these systems. This is supported by results from our isothermal and adiabatic decompression rhyolite-MELTS simulations (Fig. 15): they show that the differences in the initial depth (and thus the liquidus temperatures) for these systems leads to substantially more crystallization of Taupo than Oruanui during decompression. Consequently, even if the ascent time was comparable for these systems, the Taupo magma likely incurred greater undercooling than Oruanui, resulting in faster crystallization and more microlite nucleation.

Summary

More work will be necessary to establish which, if any, of these scenarios can explain the microlite discrepancy we find. From our results, analysis, and comparisons with other systems, we find that short ascent times, slow decompression rates, a lack of stalling potential (due to shallow storage), and low liquidus temperatures were all possible in

the Oruanui system and would all serve to inhibit microlite crystallization, though not all could be in operation simultaneously (e.g., short ascent and slow decompression). While we do not have as many constraints for Taupo, the opposite conditions would promote microlite crystallization in that system, and pressure and composition data do allow for potentially longer ascent times, higher liquidus temperatures, and added opportunity for stalling during ascent. Most likely, it is a combination of these various factors, though faster decompression is not likely to have been the cause.

Comparison with other systems also allows us to make some hypotheses regarding the decompression history of the Taupo magma. Namely, that Taupo decompression rates may have been similar to those estimated for the Bishop Tuff. Further work assessing textures, compositions, and storage conditions of other large-volume magmatic systems will be important additional sources of comparison and constraint on these hypotheses.

Recent large-volume silicic magmatism at the TVC

Integrating information from crystal textures, crystal compositions, and glass compositions results in a clear picture of recent large-volume silicic magmatism at the TVC and highlights the individuality of the eruptible Oruanui and Taupo magmas: the Oruanui magma was enormous in volume, highly evolved in composition, and resided at shallow depths in the TVC crust, while the eruptible Taupo magma was smaller in volume, much less evolved in composition, and resided much deeper in the crust. The dissimilarity in microlite textures also likely reflects significant differences in the eruptive process the two systems incurred as a result of differences in their storage depths, decompression styles, and/or compositions.

Yet, despite these disparities in size, composition, storage, and eruption, phenocryst textures highlight an important similarity between these systems: they show that the final, crystal-poor magmas involved in the Oruanui and Taupo eruptions were ephemeral in the crust, residing there for strikingly similar decadal to millennial timescales. This is not a unique result, as other studies are increasingly finding similarly short timescales for these and other caldera-forming systems (e.g., Flaherty et al. 2018). However, our study of two such systems from the same volcanic center is a new contribution, and it suggests a fundamental characteristic of the recent crust and magmatism at the TVC: regardless of where they resided, large-to-giant volumes of crystal-poor silicic magma were unstable there.

In fact, given the rate and number of small-volume eruptions between these caldera-forming events, it may be that most any volume of magma was unstable at the TVC during that period of ‘hyperactivity.’ An interesting question, in turn, is what ultimately allowed (allows?) for the generation

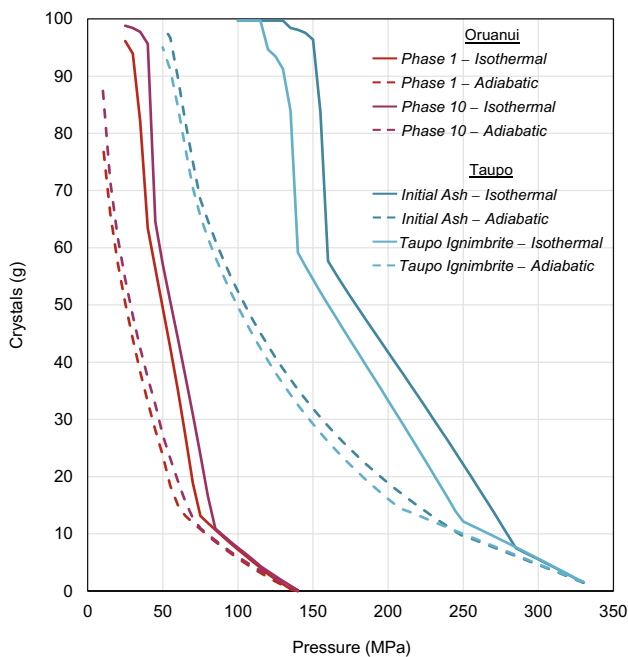


Fig. 15 Results from decompression rhyolite-MELTS simulations for isothermal (solid lines) and adiabatic (dashed lines) conditions using Taupo and Oruanui whole-rock compositions. Starting pressures were derived from rhyolite-MELTS pressures obtained in this study for glass compositions from the appropriate units. Liquidus temperatures calculated by rhyolite-MELTS for isothermal simulations are 835 °C (Oruanui Phase 1), 825 °C (Oruanui Phase 10), 761 °C (Taupo Initial Ash), and 766 °C (Taupo Ignimbrite)

of tens to hundreds of cubic kilometers of crystal-poor silicic magma volumes at the TVC? The fact that 26 smaller ($\leq 1 \text{ km}^3$) volume eruptions occurred over the short $\sim 24 \text{ ka}$ between the Oruanui and Taupo eruptions suggests that there was a significant difference in the crustal environment when these large-to-giant volumes formed. Previous work suggests that the rhyolites erupted at the TVC were generated from crystal-rich mushes (e.g., Wilson et al. 2009; Allan et al. 2017; Barker et al. 2015), and in this context our data suggest that the amount of eruptible magma that accumulates for a given eruption may be a function of how efficiently melt is extracted from that mush and/or the size of the mush, rather than the amount of time available for accumulation. Alternative paradigms for the generation of large volumes of silicic magma suggest that they are the result of high magmatic flux in the crust (e.g., Glazner et al. 2004), and Wilson et al. (2009) do note that the central TVZ experiences a particularly high magma flux. In this case, our data suggest that the high flux required to generate these volumes was episodic and relatively brief, but the duration of such episodes was similar for volumes ranging from tens to hundreds of cubic kilometers of magma. In either case, tectonics likely influenced the process, and links between magmatism and tectonics have been identified previously at the TVC: Allan et al. (2013) suggested that magma-assisted rifting boosted extraction of the Oruanui melt from a mush, and Barker et al. (2016) suggested that the post-Oruanui eruptions were motivated by new and enhanced rifting in the TVZ that was concentrated at the TVC. The fact that this enhanced rifting is hypothesized to have occurred throughout the post-Oruanui eruptive history (Barker et al. 2015, 2016), however, implies that there was something still more unique about the crustal environment of the TVC that allowed for the rapid accumulation of the unstable, large-to-giant volumes of crystal-poor high-silica rhyolite involved in the caldera-forming eruptions.

Alternatively, perhaps it is the crustal conditions alone that promote or obstruct an eruption from happening. In other words, large volume eruptions may represent a period when crustal conditions make it such that either magmas cannot erupt, and so they grow to large volumes, or eruptible magmas accumulate especially rapidly. Given that the periods preceding both the Oruanui and Taupo eruption involved significant magmatic activity (see Charlier et al. 2005), the ability for the crust to accommodate these magma volumes was likely heightened during this time, as repeated magmatic intrusions would serve to warm the crust and prime it for the accumulation of large magma volumes (e.g., Rowland et al. 2010; Gravley et al. 2016). Allan et al. (2017) also suggest that mafic magmas played an important role in triggering the Oruanui eruption, and Barker et al. (2015) suggest they heavily intruded the crust after the Oruanui eruption and during the post-Oruanui eruptive period; this would also act

as an important heat source for conditioning the crust. The convergence of these thermal conditions with tectonics at the TVC may have ultimately created the environment necessary for the accumulation of the large-to-giant eruptible magma volumes, regardless of whether these volumes existed as single or multiple magma batches. Further, in accord with the ideas that the TVC magmatic system was entirely reconstructed after the Oruanui eruption (Barker et al. 2015) and that large silicic eruptions can alter existing fault behaviors (Rowland et al. 2010), our data suggest that the depth in the crust where these conditions were achieved differed for the Oruanui and Taupo magmatic systems.

Finally, the similarity in the evolution of magma storage depth, magma composition, eruption size, and eruption frequency for caldera-forming systems in the recent TVZ and during the preceding ignimbrite ‘flare-up’ in the western central TVZ is also striking (Gravley et al. 2016; Gualda et al. 2018), and it suggests that the modern TVC may currently be in a state of flare up. This comparison further supports the idea that the TVZ crust requires priming and maturation to ultimately allow for the accumulation of enormous volumes of crystal-poor, high-silica rhyolite magma and that perhaps there is a consistent timescale and evolution in storage conditions associated with the reconstruction of these caldera-forming systems following a supereruption.

Conclusions

In this work, we combine textural and geochemical datasets to investigate the storage, longevity, and eruption of the crystal-poor, melt-rich eruptible Oruanui and Taupo magmas from the Taupo Volcanic Center, the source of the two most recent caldera-forming silicic eruptions from the Taupo Volcanic Zone. Our analysis shows that:

1. The eruptible Oruanui magma was gigantic in volume, highly evolved, and resided at shallow depths (average 50–215 MPa) in the crust. The Taupo magma was smaller, less evolved, and resided much deeper in the crust (average 290–350 MPa).
2. Phenocrysts in the crystal-poor, melt-rich magma bodies that ultimately fed these eruptions record short timescales—decades to a few millennia before the eruption. The similarity of these timescales is striking because the volumes of magma involved in these two eruptions differed by an order of magnitude. This suggests that the size of an eruption (at least of these magnitudes) is not a function of the residence time of an eruptible magma in the crust. Furthermore, the similarity of these estimates to those from other large-volume systems suggests that there is some universality to short residence times of eruptible magma and that they may be characteristic of

silicic systems that feed very large to supersized eruptions.

3. A pronounced difference in groundmass textures of Oruanui and Taupo samples indicates important differences in the conditions and processes of the eruption of these systems. Overall, Oruanui deposits are striking in their lack of microlites—this is distinct from both Taupo products and those from many other systems (e.g., Bishop Tuff, Peach Spring, Mount St. Helens). By combining timescale estimates and observations from textures, storage pressure data from geobarometry, and published data on ascent rates, we find that the textural discrepancy between the TVC systems may be a direct or indirect reflection of their storage pressures. Namely, that the difference in their storage depths resulted in different ascent durations, decompression paths, and/or level of undercooling, which affected the ultimate crystallization of microlites. We find that comparatively slow decompression of the Oruanui system, rather than fast decompression, could be a part of the explanation as well. Additional constraints on decompression and ascent for the Taupo magmatic system will be key to ultimately determining which of these explanations is/are most applicable. While our analysis is not conclusive, it paves the way for further work and highlights the power in combining textural and geochemical datasets. That's just, like, our opinion, man.
4. Comparing the evolution of storage depths and compositions of the recent TVC eruptions with those in the preceding ignimbrite 'flare-up' (Gravley et al. 2016; Gualda et al. 2018) we find a similar trend—from shallow storage of a mature system (Oruanui) to deep storage of a less mature system that forms as the magmatic system is being reconstructed (Taupo). The comparison supports the idea that the modern TVC may be flaring up (Gravley et al. 2016) and, more generally, it highlights the evolution of magma storage depths with increasing system maturity.

Acknowledgements Portions of this work were performed at GeoSoilEnviroCARS (Sector 13), Advanced Photon Source (APS), Argonne National Laboratory. GeoSoilEnviroCARS is supported by the National Science Foundation—Earth Sciences (EAR-1128799, EAPSI-1209584) and Department of Energy-GeoSciences (DE-FG02-94ER14466). This research used resources of the Advanced Photon Source, a US Department of Energy (DOE) Office of Science User Facility operated for the DOE Office of Science by Argonne National Laboratory under Contract No. DE-AC02-06CH11357. Funding was also provided by an NSF EAPSI Fellowship to K. Wright, and NSF grant EAR-1151337 to G. Gualda. Reviews by Ben Andrews and Christy Till were helpful and thought-provoking. Finally, we would like to recognize and thank Fred Anderson for sharing his samples, his time, and—most importantly—his many quiet-but-ever-clever insights over the years; we miss him.

References

- Allan ASR, Wilson CJN, Millet M-A, Wysoczanski RJ (2012) The invisible hand: tectonic triggering and modulation of a rhyolitic supereruption. *Geology* 40:563–566
- Allan ASR, Morgan DJ, Wilson CJN, Millet M-A (2013) From mush to eruption in centuries: assembly of the super-sized Oruanui magma body. *Contrib Miner Petrol* 166:143–164
- Allan ASR, Barker SJ, Millet M-A, Morgan DJ, Rooyackers SM, Schipper CI, Wilson CJN (2017) A cascade of magmatic events during the assembly and eruption of a super-sized magma body. *Contrib Miner Petrol* 172:49
- Barker SJ, Wilson CJN, Smith EGC, Charlier BLA, Wooden JL, Hiess J, Ireland TR (2014) Post-supereruption magmatic reconstruction of Taupo Volcano (New Zealand), as reflected in zircon ages and trace elements. *J Petrol* 55:1511–1533
- Barker SJ, Wilson CNJ, Allan ASR, Schipper CI (2015) Fine-scale temporal recovery, reconstruction and evolution of a post-supereruption magmatic system. *Contrib Miner Petrol* 170:5
- Barker SJ, Wilson CJN, Morgan DJ, Rowland JV (2016) Rapid priming, accumulation, and recharge of magma driving recent eruptions at a hyperactive caldera volcano. *Geology* 44:323–326
- Befus KS, Andres BJ (2018) Crystal nucleation and growth produced by continuous decompression of Pinatubo magma. *Contrib Miner Petrol* 173:92
- Bégué F, Deering CD, Gravley DM, Kennedy BM, Chambefort I, Gualda GAR, Bachmann O (2014a) Extraction, storage and eruption of multiple isolated magma batches in the paired Mamaku and Ohakuri eruption, Taupo Volcanic Zone, New Zealand. *J Petrol* 55:1653–1684
- Bégué F, Gualda GAR, Ghiorso MS, Pamukcu AS, Kennedy BM, Gravley DM, Deering CD, Chambefort I (2014b) Phase-equilibrium geobarometers for silicic rocks based on rhyolite-MELTS. Part 2: application to Taupo Volcanic Zone rhyolites. *Contrib Mineral Petrol* 168:1082
- Blundy J, Cashman K (2001) Ascent-driven crystallisation of dacite magmas at Mount St Helens, 1980–1986. *Contrib Miner Petrol* 140:631–650
- Bruegger CR, Hammer JE (2010) Crystallization kinetics in continuous decompression experiments: implications for interpreting natural magma ascent processes. *J Petrol* 51:1941–1965
- Cashman K (1988) Crystallization of Mount St. Helens 1980–1986 dacite: a quantitative textural approach. *Bull Volcanol* 50:194–209
- Cashman K, Blundy J (2000) Degassing and crystallization of ascending andesite and dacite. *Philos Trans Math Phys Eng Sci* 358:1487–1513
- Cashman K, Blundy J (2013) Petrological cannibalism: the chemical and textural consequences of incremental magma body growth. *Contrib Miner Petrol* 166:703–729
- Cashman KV, Marsh BD (1988) Crystal size distribution (CSD) in rocks and the kinetics and dynamics of crystallization II: Mākapuhi lava lake. *Contrib Miner Petrol* 99:292–305
- Charlier BLA, Wilson CJN, Lowenstern JB, Blake S, Van Calsteren PW, Davison JP (2005) Magma generation at a large, hyperactive silicic volcano (Taupo, New Zealand) revealed by U–Th and U–Pb systematics in zircons. *J Petrol* 46:3–32
- Charlier BLA, Wilson CJN, Davidson JP (2008) Rapid open-system assembly of a large silicic magma body: time-resolved evidence from cored plagioclase crystals in the Oruanui eruption deposits, New Zealand. *Contrib Miner Petrol* 156:799–813
- Cherniak DJ, Watson EB, Wark DA (2007) Ti diffusion in quartz. *Chem Geol* 236:65–74
- Cooper KM, Kent AJR (2014) Rapid remobilization of magmatic crystals kept in cold storage. *Nature* 506:480–483

- Cooper GF, Wilson CJN, Millet M-A, Baker JA, Smith EGC (2012) Systematic tapping of independent magma chambers during the 1 Ma Kidnappers supereruption. *Earth Planet Sci Lett* 313–314:23–33
- Couch S, Sparks RSJ, Carroll MR (2003) The kinetics of degassing-induced crystallization at Soufrière Hills volcano, Montserrat. *J Petrol* 44:1477–1502
- Druitt TH, Costa F, Deloule E, Dungan M, Scaillet B (2012) Decada to monthly timescales of magma transfer and reservoir growth at a caldera volcano. *Nature* 482:77–80. <https://doi.org/10.1038/nature10706>
- Dunbar NW, Kyle PR (1993) Lack of volatile gradient in the Taupo plinian-ignimbrite transition: evidence from melt inclusion analysis. *Am Miner* 78:612–618
- Dunbar NW, Hervig RL, Kyle PR (1989a) Determination of pre-eruptive H₂O, F and Cl contents of silicic magmas using melt inclusions: examples from Taupo volcanic center, New Zealand. *Bull Volcanol* 51:177–184
- Dunbar NW, Kyle PR, Wilson CJN (1989b) Evidence for limited zonation in silicic magma systems, Taupo Volcanic Zone, New Zealand. *Geology* 17:234–236
- Eberhart-Phillips D, Reyners M, Chadwick M, Stuart G (2008) Three-dimensional attenuation structure of the Hikurangi subduction zone in the central North Island, New Zealand. *Geophys J Int* 174:418–434
- Flaherty T, Druitt TH, Tuffen H, Higgins MD, Costa F, Cadoux A (2018) Multiple timescale constraints for high-flux magma chamber assembly prior to the Late Bronze Age eruption of Santorini (Greece). *Contrib Miner Petrol* 173:75
- Gelman SE, Deering CD, Gutierrez FJ, Bachmann O (2013) Evolution of the Taupo Volcanic Center, New Zealand: petrological and thermal constraints from the Omega dacite. *Contrib Miner Petrol* 166:1355–1374
- Ghiorso MS, Gualda GAR (2015) An H₂O–CO₂ mixed fluid saturation model compatible with rhyolite-MELTS. *Contrib Miner Petrol* 169:53
- Glazner AF, Barley JM, Coleman DS, Gray W, Taylor RZ (2004) Are plutons assembled over millions of years by amalgamation from small magma chambers? *GSA Today* 14:4–11
- Gravley DM, Wilson CJN, Leonard GS, Cole JW (2007) Double trouble: paired ignimbrite eruptions and collateral subsidence in the Taupo Volcanic Zone, New Zealand. *GSA Bull* 119:18–30
- Gravley DM, Deering CD, Leonard GS, Rowland JV (2016) Ignimbrite flare-ups and their drivers: a New Zealand perspective. *Earth Sci Rev* 162:65–82
- Gualda GAR, Ghiorso MS (2013) The Bishop Tuff giant magma body: an alternative to the Standard Model. *Contrib Miner Petrol* 166:755–775
- Gualda GAR, Ghiorso MS (2014) Phase-equilibrium geobarometers for silicic rocks based on rhyolite-MELTS. Part 1: principles, procedures, and evaluation of the method. *Contrib Mineral Petrol* 168:1033
- Gualda GAR, Rivers M (2006) Quantitative 3D petrography using X-ray tomography: application to Bishop Tuff pumice clasts. *J Volcanol Geotherm Res* 154:48–62
- Gualda GAR, Sutton SR (2016) The year leading to a supereruption. *PLoS One* 11:e0159200
- Gualda GAR, Cook DL, Chopra R, Qin L, Anderson AT, Rivers ML (2004) Fragmentation, nucleation and migration of crystals and bubbles in the Bishop Tuff rhyolitic magma. *Earth Environ Sci Trans R Soc Edinb* 95:375–390
- Gualda GAR, Pamukcu AS, Claiborne LL, Rivers ML (2010) Quantitative 3D petrography using X-ray tomography 3: documenting accessory phases with differential absorption tomography. *Geosphere* 6:782–792
- Gualda GAR, Pamukcu AS, Ghiorso MS, Anderson AT, Sutton SR, Rivers ML (2012) Timescales of quartz crystallization and the longevity of the Bishop giant magma body. *PLoS One* 7:e37492
- Gualda GAR, Gravley DM, Connor M, Hollman B, Pamukcu AS, Bégué F, Ghiorso MS, Deering CD (2018) Climbing the crustal ladder: magma storage-depth evolution during a volcanic flare-up. *Sci Adv* 4:eaap7567
- Gualda GAR, Bégué F, Pamukcu AS, Ghiorso MS (2019) Rhyolite-MELTS vs DERP—Newer does not make it better: a comment on ‘The effect of anorthite content and water on quartz-feldspar cotectic compositions in the rhyolitic system and implications for geobarometry’ by Wilke et al. (2017; *Journal of Petrology*, 58, 789–818). *J Petrol* 60:855–864
- Hammer JE, Rutherford MJ (2002) An experimental study of the kinetics of decompression-induced crystallization in silicic melt. *J Geophys Res* 107:2021
- Hammer JE, Cashman KV, Hoblitt RP, Newman S (1999) Degassing and microlite crystallization during pre-climactic events of the 1991 eruption of Mt. Pinatubo, Philippines. *Bull Volcanol* 60:355–380
- Heise W, Bibby HM, Caldwell TG, Bannister SC, Ogawa Y, Takakura S, Uchida T (2007) Melt distribution beneath a young continental rift: the Taupo Volcanic Zone. *N Z Geophys Res Lett* 34:L14313
- Hogg A, Lowe DJ, Palmer J, Boswijk G, Ramsey CB (2012) Revised calendar date for the Taupo eruption derived by ¹⁴C wiggle-matching using a New Zealand kauri ¹⁴C calibration data set. *Holocene* 22:439–449. <https://doi.org/10.1177/0959683611425551>
- Hort M (1998) Abrupt change in magma liquidus temperature because of volatile loss or magma mixing: effects on nucleation, crystal growth and thermal history of the magma. *J Petrol* 39:1063–1076
- Houghton BF, Carey RJ, Cashman KV, WilsonHobden CJNBJ, Hammer JE (2010) Diverse patterns of ascent, degassing, and eruption of rhyolite magma during the 1.8 ka Taupo eruption, New Zealand: evidence from clast vesicularity. *J Volcanol Geotherm Res* 195:31–47
- Johannes W, Holtz F (1996) Petrogenesis and experimental petrology of granitic rocks. *Minerals and rocks series*, vol 22. Springer, Berlin
- Ketcham RA (2005) Computational methods for quantitative analysis of three-dimensional features in geological specimens. *Geosphere* 1:32–41
- Leeman WP, MacRae CM, Wilson NC, Torpy A, Lee C-TA, Student JJ, Thomas JB, Vicenzi EP (2012) A study of cathodoluminescence and trace element compositional zoning in natural quartz from volcanic rocks: mapping titanium content in quartz. *Microsc Microanal* 18:1322–1341
- Liu Y, Anderson AT, Wilson CJN, Davis AM, Steele IM (2006) Mixing and differentiation in the Oruanui rhyolitic magma, Taupo, New Zealand: evidence from volatiles and trace elements in melt inclusions. *Contrib Mineral Petrol* 151:71–87
- Liu Y, Anderson AT, Wilson CJN (2007) Melt pockets in phenocrysts and decompression rates of silicic magmas before fragmentation. *J Geophys Res Solid Earth* 112:B06204
- Manville V, Wilson CJN (2004) The 26.5 ka Oruanui eruption, New Zealand: a review of the roles of volcanism and climate in the post-eruptive sedimentary response. *N Z J Geol Geophys* 47:525–547
- Marsh BD (1988) Crystal size distribution (CSD) in rocks and the kinetics and dynamics of crystallization. *Contrib Miner Petrol* 99:277–291
- Marsh BD (1998) On the interpretation of crystal size distributions in magmatic systems. *J Petrol* 39:553–599
- Matthews NE, Huber C, Pyle DM, Smith VC (2012) Timescales of magma recharge and reactivation of large silicic systems from Ti diffusion in quartz. *J Petrol* 53:1385–1416

- Myers ML, Wallace PJ, Wilson CJN (2018) Inferring magma ascent timescales and reconstructing conduit processes in explosive rhyolitic eruptions using diffusive losses of hydrogen from melt inclusions. *J Volcanol Geotherm Res* 369:95–112
- Pamukcu AS, Gualda GAR (2010) Quantitative 3D petrography using X-ray tomography 2: combining information at various resolutions. *Geosphere* 6:775–781
- Pamukcu AS, Gualda GAR, Anderson AT (2012) Crystallization stages of the Bishop Tuff magma body recorded in crystal textures in pumice clasts. *J Petrol* 53:589–609
- Pamukcu AS, Carley TL, Gualda GAR, Miller CF, Ferguson CA (2013) The evolution of the Peach Spring giant magma body: evidence from accessory mineral textures and compositions, bulk pumice and glass geochemistry, and rhyolite-MELTS modeling. *J Petrol* 54:1109–1148
- Pamukcu AS, Gualda GAR, Ghiorso MS, Miller CF, McCracken RG (2015a) Phase-equilibrium geobarometers for silicic rocks based on rhyolite-MELTS—part 3: application to the Peach Spring Tuff (Arizona-California-Nevada, USA). *Contrib Miner Petrol* 169:33
- Pamukcu AS, Gualda GAR, Begue F, Gravley DM (2015b) Melt inclusion shapes: timekeepers of short-lived giant magma bodies. *Geology* 43:947–950
- Pamukcu AS, Ghiorso MS, Gualda GAR (2016) High-Ti, bright-CL rims in volcanic quartz: a result of very rapid growth. *Contrib Miner Petrol* 171:105
- Rivers ML, Sutton SR, Eng PJ (1999) Geoscience applications of X-ray computed microtomography. In: *Proceedings of SPIE 3772, developments in X-ray Tomography II*
- Rowland JV, Wilson CJN, Gravley DM (2010) Spatial and temporal variations in magma-assisted rifting, Taupo Volcanic Zone, New Zealand. *J Volcanol Geotherm Res* 190:89–108
- Rubin AE, Cooper KM, Till CB, Kent AJR, Costa F, Bose M, Gravley DM, Deering CD, Cole J (2017) Rapid cooling and cold storage in a silicic magma reservoir recorded in individual crystals. *Science* 356:1154–1156
- Salisbury MJ, Bohron WA, Clynne MA, Ramos FC, Hoskin P (2008) Multiple plagioclase populations identified by crystal size distribution and in situ chemical data: Implications for timescales of magma chamber processes associated with the 1915 eruption of Lassen Peak, CA. *J Petrol* 49:1755–1780
- Saunders KE (2009) Micro-analytical studies of the petrogenesis of silicic arc magmas in the Taupo Volcanic Zone and southern Kermadec Arc, New Zealand
- Schmitt AK, Danisik M, Evans NJ, Siebel W, Kiemele E, Aydin F, Harvey JC (2011) *Contrib Mineral Petrol* 162:1215–1231
- Seitz S, Putlitz B, Baumgartner LP, Escrig S, Meibom A, Bouvier A-S (2016) Short magmatic residence times of quartz phenocrysts in Patagonian rhyolites associated with Gondwana breakup. *Geology* 44:67–70. <https://doi.org/10.1130/G37232.1>
- Self S, Sparks RSJ (1978) Characteristics of widespread pyroclastic deposits formed by the interaction of silicic magma and water. *Bull Volcanol* 41:196
- Smith RT, Houghton BF (1995) Delayed deposition of plinian pumice during phreatoplinian volcanism: the 1800-year-B.P. Taupo eruption, New Zealand. *J Volcanol Geotherm Res* 67:221–226
- Smith VC, Shane P, Nairn IA (2005) Trends in rhyolite geochemistry, mineralogy, and magma storage during the last 50 kyr at Okataina and Taupo volcanic centres, Taupo Volcanic Zone, New Zealand. *J Volcanol Geotherm Res* 148:372–406
- Sutton AN, Blake S, Wilson CJN (1995) An outline geochemistry of rhyolite eruptives from Taupo volcanic centre, New Zealand. *J Volcanol Geotherm Res* 68:153–175
- Sutton AN, Blake S, Wilson CJN, Charlier BLA (2000) Late Quaternary evolution of a hyperactive rhyolite magmatic system: Taupo volcanic centre, New Zealand. *J Geol Soc* 157:537–552
- Szymanowski D, Wotzlaw J-F, Ellis BS, Bachmann O, Guillong M, von Quadt A (2017) Protracted near-solidus storage and pre-eruptive rejuvenation of large magma reservoirs. *Nat Geosci* 10:777–782
- Tuttle OF, Bowen NL (1958) Origin of granite in the light of experimental studies in the system $\text{NaAlSi}_3\text{O}_8\text{--KAlSi}_3\text{O}_8\text{--SiO}_2\text{--H}_2\text{O}$. *GSA Mem* 74:1–145.
- Vandergoes MJ, Hogg AG, Lowe DJ, Newnham RM, Denton GH, Southon J, Barrell DJA, Wilson CJN, McGlone MS, Allan ASR, Almond PC, Petchey F, Dabell K, Dieffenbacher-Krall AC, Blaauw M (2013) A revised age for the Kawakawa/Oruanui tephra, a key marker for the Last glacial maximum in New Zealand. *Quat Sci Rev* 74:195–201
- Wark DA, Watson EB (2006) Titanite: a titanium-in-quartz geothermometer. *Contrib Miner Petrol* 152:743–754
- Wilke S, Hotlz F, Neave DA, Almeev R (2017) The effect of anorthite content and water on quartz-feldspar cotectic compositions in the rhyolitic system and implications for geobarometry. *J Petrol* 58:789–818
- Wilson CJN (1993) Stratigraphy, chronology, styles and dynamics of late quaternary eruptions from Taupo volcano, New Zealand. *Philos Trans R Soc Lond Ser A Phys Eng Sci* 343:205–306
- Wilson CJN (2001) The 26.5 ka Oruanui eruption, New Zealand: an introduction and overview. *J Volcanol Geotherm Res* 112:133–174
- Wilson CJN, Charlier BLA (2009) Rapid rates of magma generation at contemporaneous magma systems, Taupo Volcano, New Zealand: insights from U–Th model-age spectra in zircons. *J Petrol* 50:875–907
- Wilson CJN, Walker GPL (1982) Ignimbrite depositional facies: the anatomy of a pyroclastic flow. *J Geol Soc* 139:581–592
- Wilson CJN, Walker GPL (1985) The Taupo eruption, New Zealand I. General aspects. *Philos Trans R Soc Lond Ser A Math Phys Sci* 314:199–228
- Wilson CJN, Ambraseys NN, Bradley J, Walker GPL (1980) A new date for the Taupo eruption, New Zealand. *Nature* 188:252–253
- Wilson CJN, Houghton BF, McWilliams MO, Lanphere MA, Weaver SD, Briggs RM (1995) Volcanic and structural evolution of Taupo Volcanic Zone, New Zealand: a review. *J Volcanol Geotherm Res* 68:1–28
- Wilson CJN, Blake S, Charlier BLA, Sutton AN (2006) The 26.5 ka Oruanui eruption, Taupo Volcano, New Zealand: Development, characteristics and evacuation of a large rhyolitic magma body
- Wilson CJN, Gravley DM, Leonard GS, Rowland JV (2009) Volcanism in the central Taupo Volcanic Zone, New Zealand: Tempo, styles and controls. In: Thordarson T, Self S, Larsen G, Rowland SK, Hoskuldsson A (eds) *Studies in volcanology: the legacy of George Walker*. Special Publications of IAVCEI, vol 2. pp 225–247
- Zellmer GF, Clavero JE (2006) Using trace element correlation patterns to decipher a sanidine crystal growth chronology: an example from Taapaca volcano, Central Andes. *J Volcanol Geotherm Res* 156:291–301

Publisher's Note Springer Nature remains neutral with regard to jurisdictional claims in published maps and institutional affiliations.